Wastewater-based estimation of the effective reproductive number of SARS-CoV-2

Authors: Jana S. Huisman (1,2,3*), Jérémie Scire (2,3), Lea Caduff (4), Xavier Fernandez-Cassi (5), Pravin Ganesanandamoorthy (4), Anina Kull (4), Andreas Scheidegger (4), Elyse Stachler (4), Alexandria B. Boehm (6), Bridgette Hughes (7), Alisha Knudson (7), Aaron Topol (7), Krista R. Wigginton (8), Marlene K. Wolfe (6), Tamar Kohn (5,†), Christoph Ort (4,†), Tanja Stadler (2,3,†), Timothy R. Julian (4,9,10,†)

Affiliations

1. Department of Environmental Systems Science, ETH Zurich, Swiss Federal Institute of Technology, Zurich, CH-8092, Switzerland
2. Swiss Institute of Bioinformatics, Lausanne, CH-1015, Switzerland
3. Department of Biosystems Science and Engineering, ETH Zurich, Swiss Federal Institute of Technology, Basel, CH-4058, Switzerland
4. Eawag, Swiss Federal Institute of Aquatic Science and Technology, Dübendorf, CH-8600, Switzerland
5. Laboratory of Environmental Chemistry, School of Architecture, Civil and Environmental Engineering, École Polytechnique Fédérale de Lausanne (EPFL), Lausanne, CH-1015, Switzerland
6. Department of Civil and Environmental Engineering, Stanford University, Stanford, 94305, California, United States of America
7. Verily Life Sciences, South San Francisco, 94080, California, United States of America
8. Department of Civil and Environmental Engineering, University of Michigan, Ann Arbor 48109, Michigan, United States of America
9. Swiss Tropical and Public Health Institute, Basel, CH-4051, Switzerland
10. University of Basel, Basel, CH-4055, Switzerland

†These authors contributed equally
*Corresponding author: jana.huisman@env.ethz.ch

Classification: Biological Sciences, Environmental sciences
Key words: wastewater-based epidemiology, public health surveillance, COVID-19, sewage

Abstract:

The effective reproductive number, Re, is a critical indicator to monitor disease dynamics, inform regional and national policies, and estimate the effectiveness of interventions. It describes the average number of new infections caused by a single infectious person through time. To date, Re estimates are based on clinical data such as observed cases, hospitalizations, and/or deaths. Here we show that the dynamics of SARS-CoV-2 RNA in wastewater can be used to estimate Re in near real-time, independent of clinical data and without associated biases stemming from clinical testing and reporting strategies. The method to estimate Re from wastewater is robust and applicable to data from different countries and wastewater matrices. The resulting estimates are as similar to the Re estimates from case report data as Re estimates based on observed cases, hospitalizations, and deaths are among each other. We further provide details on the effect of sampling frequency and the shedding load distribution on the ability to infer Re. To our knowledge, this is the first time Re has been estimated from wastewater. This method provides a low cost, rapid, and independent way to inform SARS-CoV-2 monitoring during the ongoing pandemic and is applicable to future wastewater-based epidemiology targeting other pathogens.

Significance statement:

The effective reproductive number, Re, is widely used during the COVID-19 pandemic to track disease dynamics, inform regional and national policies, and estimate the effectiveness of interventions. Re is typically estimated from clinical case data, and can be biased by e.g. changes in testing and reporting. We show longitudinal measurements of SARS-CoV-2 RNA in wastewater can be used to estimate Re, across different regions, and provide an independent assessment of the dynamics of COVID-19. Given widespread wastewater sampling during this pandemic, these Re estimates are directly applicable as a rapid, low-cost method to inform public health policy. The method can be adapted to other pathogens, including those for which clinical data is not available.

Introduction:

A critical quantity to monitor an ongoing epidemic is the effective reproductive number Re (1–4). Re describes the average number of new infections caused by a single infectious person, at a given point in time. Typically, Re is estimated from case report data (hereafter referred to as R_{cc}), including the numbers of new clinical cases, hospitalizations, and deaths (1, 3–5). Here, we show that viral RNA concentrations measured in wastewater provide an independent data set to estimate Re (hereafter referred to as R_{ww}). This complements existing R_{cc} estimates to provide a more complete picture of transmission dynamics.

Re estimates for SARS-CoV-2 are used to inform regional and national policies (6, 7). The Re changes through time and reflects changes in the immune status of the population, policy, climate, and/or individual behaviours (1, 2). It can thus be used to estimate the effectiveness of non-pharmaceutical interventions in disease control (5, 8–11). However, R_{cc} estimates have some notable drawbacks. Most importantly, they depend on robust and accurate clinical case surveillance and reporting. Temporal changes in testing capacity, hospitalisation criteria, or the definition of COVID-19-related deaths can bias the R_{cc} estimates (1, 12). These estimates are also inferred with a delay: R_{cc} is estimable once the infections occurring on that day tested positive and were reported as clinical cases (1, 2). Knowledge of this delay is necessary to accurately infer R_{cc}, yet differs through time and space, thus limiting comparability across geographic regions. Wastewater data may provide an advantage over clinical case data in all these aspects.

SARS-CoV-2 RNA measurements in wastewater can be used to understand COVID-19 epidemiology because infected individuals shed the virus into the sewer system throughout their infection. During the COVID-19 pandemic, SARS-CoV-2 RNA has been repeatedly detected in wastewater and sewage sludge globally (13–19), and measured RNA concentrations or loads correlate with clinical case data (13–15, 17). Detection of SARS-CoV-2 RNA in the wastewater implies there is at least one actively shedding infected person in the catchment served by the sewer system. Compared to clinical testing, substantially fewer wastewater samples are required to track changes in infection incidence at the community level. Wastewater data has also been integrated into compartmental models of infectious disease transmission, allowing estimation of epidemiological parameters including incidence and the basic reproductive number R0 (20, 21). Model results generally fall within the confidence intervals of estimates based on clinical case data, supporting the use of SARS-CoV-2 RNA measurements in wastewater to inform disease transmission dynamics.

Models relating SARS-CoV-2 RNA in wastewater to incidence or transmission rates are driven by assumptions of virus excretion rates into the sewer system. Excretion (via feces, saliva, and/or sputum) varies by individual and through time after infection. Generally, this can be described using a shedding load profile, which captures both the temporal dynamics of shedding (in the shedding load distribution; SLD), and the total amount of virus shed by an infected individual. Clinical studies in various settings have measured shedding from symptom onset onwards. Notable examples include Wölfel et al., who measured virus concentrations in the stool of hospitalised patients (21, 22) and Han et al., who included symptomatic and

asymptomatic children (23). Benefield et al. combined such studies into a systematic review of SARS-CoV-2 viral loads (24). However, little is known about shedding prior to symptom onset. Given uncertainty and variation in estimates of SLDs, modeling approaches to relate wastewater to transmission have varied. For example, Kaplan et al. used an infectivity profile (based on virus concentrations in the upper and lower respiratory tract from Li et al.) rather than information on gastrointestinal shedding to estimate the basic reproductive number R0 from wastewater data (20, 25). More work is needed to determine both the SLD and the amount of virus shed during an infection to relate SARS-CoV-2 RNA measurements in wastewater to epidemiology.

We measure SARS-CoV-2 RNA in sewage sludge or wastewater from two distinct monitoring programs (Zurich, Switzerland and Bay Area, CA, USA), use the measured RNA to estimate R_{ww}, and compare the estimates to R_{cc} obtained from clinical case data. We further determine the SLD that optimises the fit between R_{ww} and R_{cc} and compare it to previously reported SLDs. We find that R_{ww} is a useful metric to monitor the transmission dynamics of SARS-CoV-2, independent from clinical case data. To our knowledge, this is the first time Re has been estimated from pathogen concentrations in wastewater.

Results:

SARS-CoV-2 RNA in Wastewater. We tracked SARS-CoV-2 RNA concentrations in Zurich, Switzerland and San Jose, California, USA during a rise and fall in clinical COVID-19 cases (Fig. 1A,B; Fig. 2A,B). Data from Zurich were used to develop and assess R_{ww} estimates, and data from San Jose were used to assess the generalizability of the approach.

In Zurich, SARS-CoV-2 N1 and N2 markers of the N gene were detectable in the raw influent samples from the Zurich wastewater treatment plant between 1 September 2020 and 20 January 2021 in all 105 samples collected (Fig. 1A). Of these, 102 were above the limit of quantification. Concentrations were multiplied by daily flow rate to estimate total number of gene copies shed by people within the catchment per day (hereafter referred to as loads), resulting in median [range] loads of 13.4 [<12 (limit of detection), 13.7] $\log_{10}$ gene copies per day (gc/day) (Fig. 1A). Only one sample (29 October) was excluded based on quality control, which included monitoring sample inhibition and consistency of effluent pepper mild mottle virus (PMMoV) loads (see Supplemental Material).

In San Jose, SARS-CoV-2 N, S, and ORF1a genes were quantifiable in the settled solids of the primary settling tank in all 125 samples collected between 15 November 2020 and 19 March 2021 (Fig. 2A). The median [range] concentrations were 4.9 [3.4, 6.0], 5.0 [3.9, 6.0], and 5.0 [3.8, 6.0] $\log_{10}$ gene copies per gram dry weight (gc/g-dry weight) for N, S, and ORF1a genes, respectively (Fig. 2A). Two samples (03 January, 18 February) were excluded based on quality control using consistency of PMMoV concentrations (see Supplemental Material).

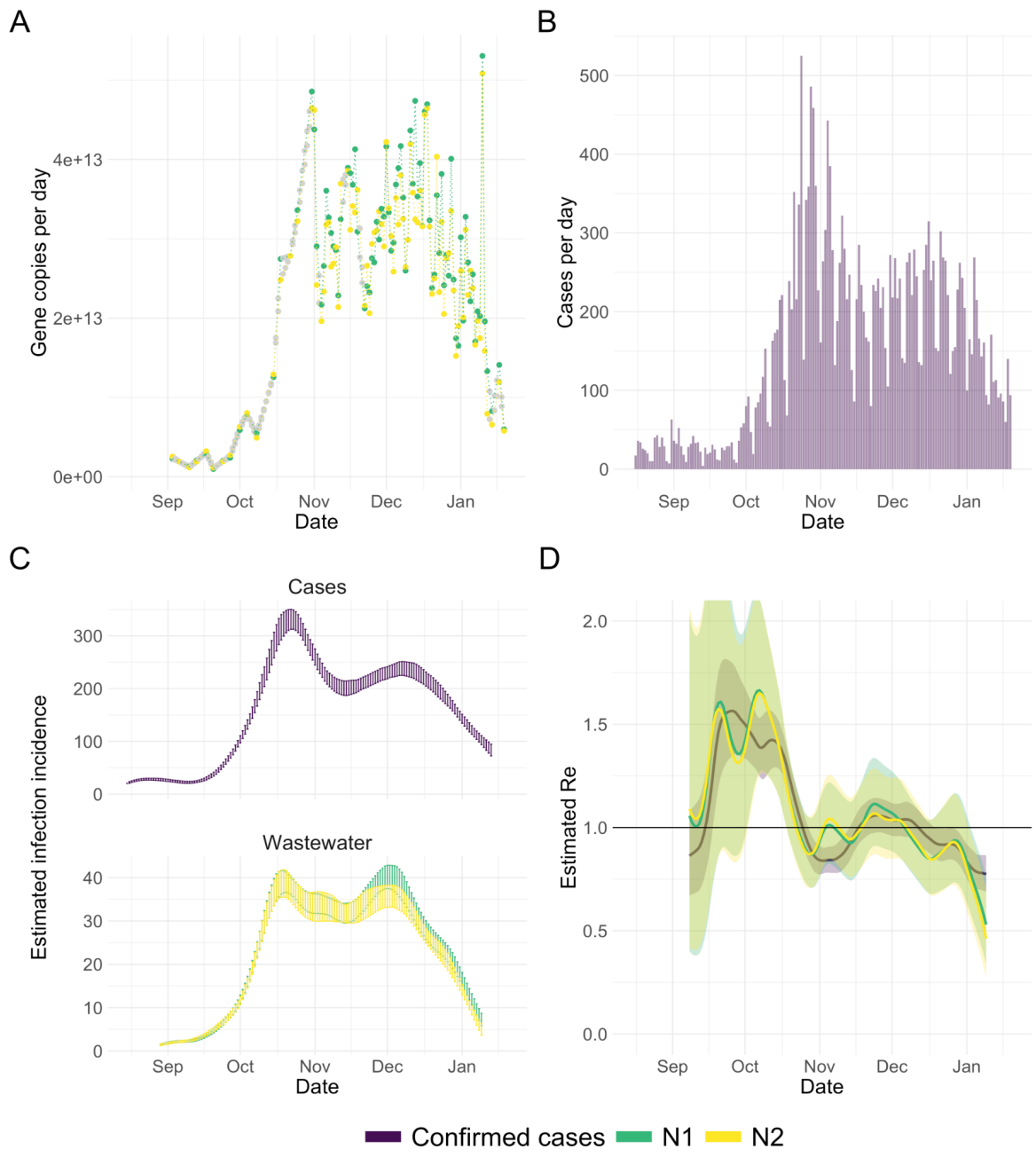

Fig. 1: R_{ww} estimation from Zurich (CHE) wastewater measurements. (A) Measured RNA loads of the N1 and N2 markers (green and yellow respectively) between 1 September 2020 and 20 January 2021. Imputed values are indicated in grey. (B) Confirmed cases (purple) in the catchment during the same time period. (C) The estimated time series of infection incidence from case reports (top), and normalised RNA loads of the N1 and N2 markers (bottom; green and yellow respectively). The measured loads were normalised by the lowest measured value (N*M = 9.7*10^11 gc per infection; see Methods). The bars indicate the mean ± standard deviation across 50 bootstrap replicates. (D) The estimated R_{ww} compared to the R_{cc} from confirmed cases. The coloured line indicates the point estimate on the original data, and the ribbons the 95% confidence interval across 50 bootstrap replicates.

Infection incidence dynamics can be inferred from wastewater measurements. Next, we related the RNA measurements in wastewater to the original infection incidence by applying a deconvolution with the shedding load distribution (see Methods). SARS-CoV-2 wastewater measurements reflect the cumulative contributions of all infected individuals actively shedding virus into the wastewater. The amount of virus shed by each individual varies through time after infection, and is captured in the shedding load profile. In general, this profile contains information about the timing of viral shedding - the shedding load distribution (SLD; which sums to 1) - and the total amount of virus shed - captured by a normalisation factor *N*. To estimate the true number of infections in the sewer shed it is important to estimate the exact value of the normalisation factor N, as well as a factor M describing losses along the way from shedding to sample processing. However, to estimate Re it suffices to know the temporal dynamics of shedding and infection (see Methods). As a first approximation, we assumed individuals do not shed prior to symptom onset, and thereafter shed according to the gastrointestinal SLD reported by Benefield et al. (24). With this assumption, we found that the dynamics of infection incidence inferred from wastewater measurements in Zurich are similar to the dynamics inferred from clinical case data (Fig. 1C). We later test the sensitivity of our results to the assumed SLD and normalisation.

The effective reproductive number R_{ww} can be estimated from RNA measurements in wastewater. We used the inferred time series of infection incidence from SARS-CoV-2 RNA measured in wastewater to estimate R_{ww} in Zurich (Fig. 1D; see Methods). There is a good correspondence between R_{ww} and R_{cc}. In fact, the average root mean squared error (RMSE) between R_{ww} and R_{cc} is 0.11 and 0.12 for N1 and N2 respectively. This is smaller than the RMSE between the Re estimates based on different sources of case report data: 0.13 between confirmed cases and hospitalisations; and 0.26 between confirmed cases and deaths (estimated on case report data from canton Zurich, which has a population 3.4x the size of the catchment, for the same time period as R_{ww}).

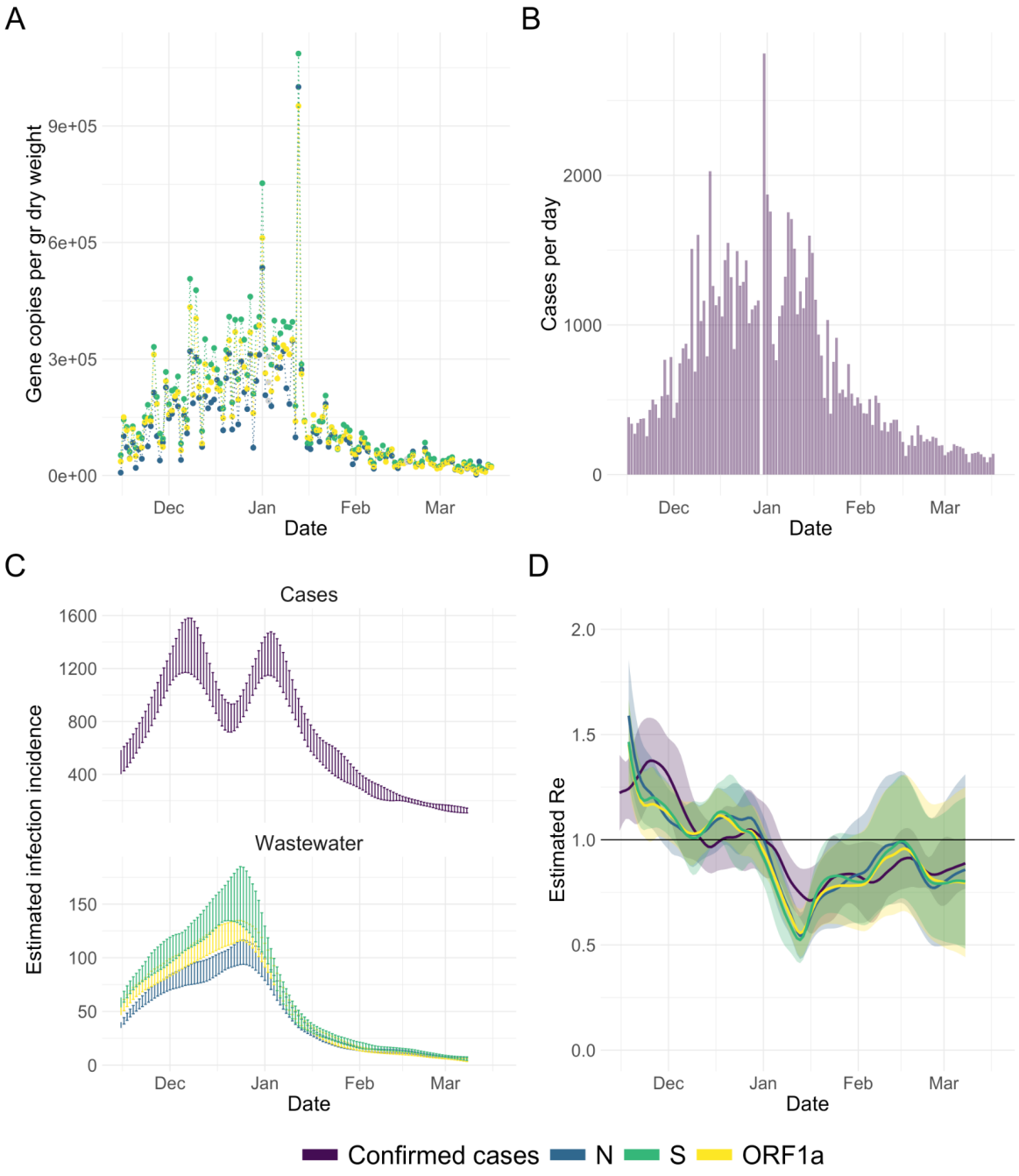

Fig. 2: R_{ww} estimation from San Jose (USA) sludge measurements: (A) Measured RNA concentrations of the N, S and ORF1a genes (blue, green, yellow respectively) between 15 November 2020 and 19 March 2021. (B) Confirmed cases in Santa Clara county (purple) during the same time period. (C) The estimated time series of infection incidence from case reports (top) and normalised RNA concentrations (bottom). The gene copies per gram dry weight were normalised by the lowest measured value (N*M = 2663.7 gc/g per infection; see Methods). The bars indicate the mean ± standard deviation across 50 bootstrap replicates. (D) The estimated R_{ww} compared to R_{cc} from confirmed cases. The coloured line indicates the point estimate on the original data, and the ribbons the 95% confidence interval across 50 bootstrap replicates.

R_{ww} can be estimated from independent data sources and different wastewater matrices. To test whether these results could be generalised to different geographic locations and wastewater matrices, we analysed daily-sampled primary sewage sludge data from the San Jose wastewater treatment plant in California.

In San Jose, the inferred infection incidence curves between confirmed cases and wastewater data follow similar trends (Fig. 2C). However, confirmed cases rise rapidly reaching a maximum and fluctuating at a plateau throughout December, whereas wastewater estimates continue to rise more gradually throughout this period (Fig. 2C). This difference is likely due to underreporting of cases during the holidays, as the testing-adjusted cases followed a trend more similar to the wastewater measurements (Fig. S1A). Starting in late December, both wastewater and cases show a similarly rapid decrease.

We found that R_{ww} agreed with R_{cc}, although there is some temporal lag between both time series (Fig. 2D). In general, both R_{ww} or R_{cc} could be inaccurately placed in time: e.g. because the SLD does not optimally capture the shedding dynamics, or because reporting delays for the clinical cases changed during the observation period. In this case, it seems likely that the R_{cc} estimates are biased by underreporting and increased testing delays. Re estimates based on the cases adjusted for testing show results more comparable to R_{ww}, especially in November/December (Fig. S1B). Furthermore, there are substantially larger differences between R_{cc} estimated using different methods (as reported on the website of the California State Department of Public Health), than between the wastewater and the confirmed case trace estimated using the same pipeline (Fig. S2).

Minimal Frequency of Wastewater Sampling needed to inform R_{ww}. While designing wastewater-based epidemiology studies, an important cost-benefit trade-off centers around the frequency of sampling. We subsampled the daily sampled wastewater measurements in Zurich and San Jose, prior to the Re estimation pipeline, to determine how this would affect the estimated R_{ww}. We assessed a range of sampling strategies that differed in the number and identity of the days sampled (e.g. Mon-Wed-Fri or Tue-Fri). For Zurich, we restricted ourselves to the period with daily sampling (22 November 2020 to 11 January 2021). Using the RMSE to quantify the similarity between different R_{ww} estimates, we found that subsampling down to 3 measurements per week still leads to results comparable to a daily sampling regime (Fig. S3, Table S1, Table S2). However, below this frequency the representativity of the R_{ww} estimate starts to depend on which days were sampled.

Susceptibility of R_{ww} estimates to the shedding load distribution. We showed that Re can be estimated from RNA measurements in wastewater, given an assumption for the SLD. However, there is substantial variation between SLDs described in the literature, across patients, bodily fluids, and geographic locations. The shape of the SLD, in particular the mean of the gamma distribution used, affects the inferred timing of peak infection incidence (Fig. S4). In our pipeline we also observe an influence of the normalisation factor N*M on the amplitude of the estimated R_{ww} (Fig. S5). In principle, the inference of the Re point estimate from an infection incidence is agnostic to the magnitude of this incidence (2, 4). However, the noise model and

deconvolution algorithm in our pipeline were optimised for data on the scale of infections per day. Here, we have chosen to normalise the wastewater measurements such that the considered gene loads are on that same scale, since R_{ww} otherwise reacts too strongly to changes in the daily incidence (Fig. S5).

Estimation of the shedding load distribution that optimizes the fit between clinical and wastewater data. Instead of assuming a single SLD and estimating R_{ww} based only on that distribution, we also asked which SLD would maximise the similarity between the R_{ww} and R_{cc} estimates. We numerically scanned across different SLDs and quantified the resulting goodness of fit between the R_{ww} and R_{cc} for both Zurich and San Jose. We assumed the SLD is described by a single gamma distribution, starting at infection, and searched for the optimal fit on a grid of mean-standard deviation parameter pairs (Table 1, Fig. 3). The fit was quantified using the root mean squared error (RMSE), coverage, and mean absolute percentage error (MAPE; see Methods).

The optimal fits based on these metrics suggest that the SLD has a mean between 7-11 days in Zurich and 5-7 days in San Jose, with a very low standard deviation of 0.5 days in both locations (Table 1). However, there is some non-identifiability in our analysis, with most optimal value pairs lying along a ridge (Figs. 3, S6, S7). This ridge corresponds to SLDs with a similar median, which result in nearly indistinguishable R_{ww} estimates (Fig. S8). If we consider the parameters yielding a fit within 10% from the optimum, the parameter ranges found in both locations are compatible and jointly suggest an SLD with mean between 6-9 days, and standard deviation between 0.5-3 days. Longer time series and more locations would further constrain this distribution. Compared to the delay between infection and case reporting, the SLD introduces a similar or lower mean delay to R_{ww}. For Zurich, the cases were delayed with respect to infection by 8.1 days on average (see Methods), which is comparable to the 6-9 days for R_{ww}. For San Jose, instead, the delay distribution of the case report data had a mean of 9.8 days. There, the wastewater may lead the confirmed cases by 1-4 days, if the current testing and reporting regime is upheld.

To compare against published SLDs, which are frequently parameterized from symptom onset instead of infection, we conducted a second analysis. Here we assumed individuals do not shed during their incubation period and subsequently shed with a gamma distribution, starting at symptom onset. In this case, we find optimal SLDs with a mean between 0.5-3 days for San Jose and 3.5-5.5 days for Zurich (Table S3, Fig. S9). These optimal distributions have a lower mean than the SLD reported by Benefield et al. (mean 6.7 days), and Han et al. (mean 4.7 days, see Methods) (23, 24). If we add the mean incubation period (5.3 days) to the results of this scan, we find that for both locations the mean delay between infection and shedding is comparable to the mean of the SLD we estimated from infection.

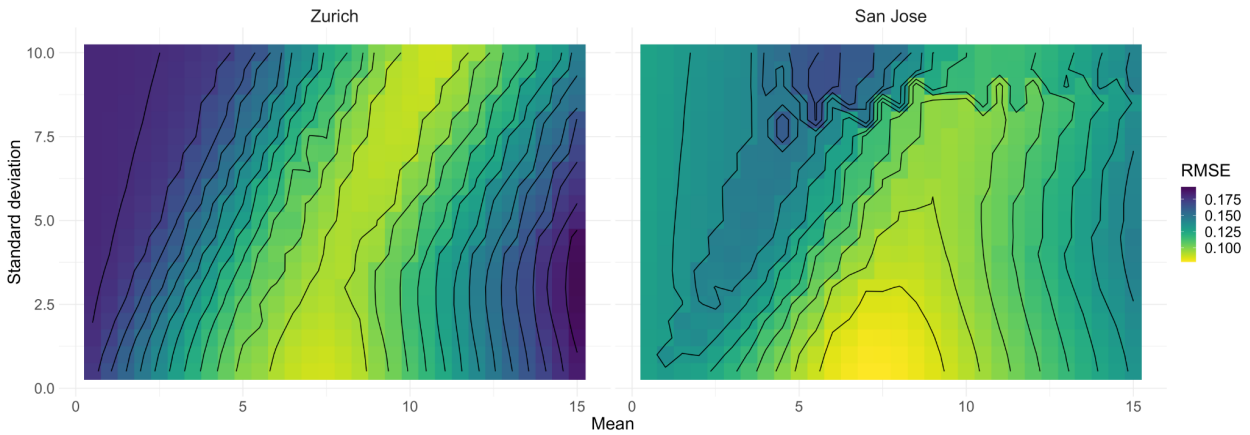

Fig. 3: RMSE between R_{cc} and R_{ww} for different shedding load distributions. We scanned across different (mean, standard deviation) parameter pairs for the SLD from time since infection. For the city of Zurich, the R_{ww} from N1 loads in wastewater was compared to that of confirmed cases in the catchment. For San Jose, we compared S gene concentrations to confirmed cases in Santa Clara County. The contour lines show SLD parameter pairs with equal RMSE, in steps of 10% of the optimum value.

Table 1: Parameters of the optimal shedding distribution from infection. We scanned across different (mean, standard deviation) parameter pairs for the SLD from time since infection. For Zurich, the Re from N1 loads in wastewater was compared to that of confirmed cases in the catchment. For San Jose, we compared S gene concentrations to confirmed cases in Santa Clara County. For all values of the scan see Figs. 3, S6, S7. All parameters are in units of days.

Comparison	Optimal pair (mean; sd)	Mean within 10% from the optimum	SD within 10% from the optimum
RMSE (Zurich)	(7.5; 0.5)	[6, 11.5]	[0.5, 10]
Coverage (Zurich)	(7; 0.5)	[6, 12.5]	[0.5, 10]
MAPE (Zurich)	(11; 10)	[6.5, 11]	[0.5, 10]
RMSE (San Jose)	(7.0; 0.5)	[6, 9]	[0.5, 3]
Coverage (San Jose)	(5; 0.5)	[1, 11]	[0.5, 10]
MAPE (San Jose)	(6; 0.5)	[5, 8]	[0.5, 2.5]

Discussion:

We showed that regular measurements of SARS-CoV-2 concentrations in wastewater and settled solids can be used to estimate the effective reproductive number Re. The variation between Re estimates from wastewater (R_{ww}) and from case report data (R_{cc}) is similar to the variation between Re estimates based on different types of case report data (clinical cases, hospitalizations, and deaths). We further showed wastewater samples should be collected at least 3 times per week to reliably estimate past R_{ww}, in line with analyses based on direct comparison of wastewater signals to clinical cases (15, 26). For real-time monitoring of R_{ww}, more frequent measurements may be preferable to ensure stable estimates when new data comes in.

Estimating R_{ww} requires accurate characterization of the SLD, i.e. the temporal dynamics of shedding. In our primary analysis, we used the distribution for gastrointestinal shedding from Benefield et al. (24). In using this SLD, we implicitly assumed that fecal shedding dominates the viral load in wastewater. However, there is a wide range in published viral shedding loads, and it is unclear which - if any - accurately capture viral shedding dynamics of people within a catchment. Virus shed in saliva, sputum, and feces are possible contributors to the total amount of virus RNA in the wastewater (27). While upper respiratory tract swabs show peak viral loads around the day of symptom onset, there are indications that sputum samples peak a few days later, and feces even after that (28–30). Studies differ in the inferred timing of peak viral load (even in the same bodily fluids), and there is a general lack of information to constrain dynamics prior to symptom onset (31). Additionally, the duration and magnitude of viral shedding seem to differ within different populations (for example, due to age or severity of disease) (32, 33). However, these individual differences will probably average out in a sufficiently large catchment and better estimates of the SLD are likely to become available as prospective sampling studies report results.

We showed that the optimal SLD can also be inferred from the fit between R_{ww} and R_{cc}. Once the SLD has been estimated from historic wastewater and case data, it may from then on provide a more accurate estimation of R_{ww}, than using one of the published SLDs. Indeed, here we show a range of SLDs inferred from our wastewater data that generally align with, but have lower means than published SLDs based on patient shedding profiles. Optimization based on alignment between R_{ww} and R_{cc} assumes accuracy of R_{cc}, which only holds when there is adequate clinical case surveillance. However, given widespread wastewater monitoring coincident to clinical case reporting, broader application of our methods would help constrain the SLD of SARS-CoV-2.

The utility of wastewater measurements for Re estimation is independent of the pipeline used to estimate Re. Here, we report results obtained with the pipeline of Huisman et al. (2). However, many estimation methods exist, differing in assumptions on smoothing, deconvolution, uncertainty quantification as well as the underlying method to estimate Re from infection incidence (1, 3, 7, 34, 35). Although the Re point estimate is agnostic to the absolute magnitude of the infection incidence (and thus comparable across wastewater treatment plants with differing sampling protocols), the rest of our pipeline - including the deconvolution and

estimation of confidence intervals - was originally developed specifically for use with clinical data. Thus, we had to normalise the measured wastewater concentrations to the same order of magnitude as the case data. Further development could make the method more specifically adapted to wastewater data, and alleviate this dependence on the normalisation.

Estimates of R_{ww} are independent of biases influencing clinical case-based estimates. R_{cc} estimates are based on only the subset of infections, hospitalizations, and/or deaths that are captured by surveillance within the healthcare system. If this subset changes, for instance due to developments in testing or reporting policy, the resulting R_{cc} estimates will be temporarily biased (2, 4). In Geneva, Switzerland, seroprevalence studies showed that the number of infections per reported case varied substantially, from an estimated 11.6 infections per reported case as of May 2020 to only 2.7 as of December 2020 (36, 37). During that period, SARS-CoV-2 RNA concentrations in wastewater better reflected the dynamics than the clinical cases (38).

However, R_{ww} estimates are also prone to biases. People's behaviours, such as defecation timing outside of a daily routine (39) and/or movement into or out of the catchment (40) can influence R_{ww} estimates, particularly when the number of infected individuals is low. RNA signals may also be impacted during sewer transport, with persistence influenced by environmental conditions (i.e., temperature) and/or sewage composition (i.e., solids content) (41–44). Furthermore, sample processing required to quantify SARS-CoV-2 RNA may introduce variation, as suggested by substantial day-to-day variation in measurements (13, 15, 38, 45). Finally, R_{ww} estimates are informed by the number and proportion of infected and/or shedding people within the catchment: if there are too few active shedders, R_{ww} may be very sensitive to the increased fluctuations in SARS-CoV-2 RNA concentrations.

Deriving Re from wastewater offers an independent method to track disease dynamics. Wastewater-based epidemiology is used globally to track the COVID-19 pandemic (https://www.covid19wbec.org/covidpoops19) (13–19). The data collected within these campaigns could be used to estimate R_{ww} with a robust method, not influenced by heterogeneous testing and reporting strategies, and hence more comparable across geographic areas. Additionally, R_{ww} estimates could be derived for the transmission of SARS-CoV-2 variants and/or other pathogens for which SLDs are known. SARS-CoV-2 variants, including Variants of Concern (VOCs), are readily detectable in wastewater (46–48) as are other pathogens (e.g., norovirus, enterovirus, hepatitis A) (49–51). This could provide the temporal, quantitative wastewater measurements needed to estimate R_{ww}. Wastewater surveillance allows estimating R_{ww} to track disease transmission dynamics in near-real time, using low cost, rapid, and geographically-comparable methods, and can be used when reporting clinical cases is not feasible, mandatory, or much delayed compared to infection and shedding.

Materials and Methods:

SARS-CoV-2 RNA quantification in wastewater (Zurich, Switzerland)

*Sample Collection and Preparation***.** From 03 September 2020 to 19 January 2021, raw influent after fine screening samples (500 ml) were collected and processed from the Werdhölzli wastewater treatment plant (Zurich, CH) to quantify SARS-CoV-2 RNA following the protocol of Fernandez-Cassi et al. 2021 (38). Samples were collected twice per week (Thursdays, Sundays) until October 29; afterwards, samples were collected almost daily. Until 25 October, samples were processed in duplicate (biological replicates).

Briefly, 24-hour flow-proportional composite samples were collected in 500 mL polystyrene or polypropylene plastic bottles, shipped on ice, and stored at 4°C for up to 8 days before processing. Aliquots (50 mL) were stirred at room temperature for 30 minutes and then clarified by sequential filtration through 2 µm glass fiber pre-filters (Merck) and 0.22 µm SteriCup filters (Merck). The filtrates were concentrated by centrifugation (3000x*g* for 30 minutes) using Centrifugal Filter Units (10kDa Centricon Plus-70, Millipore, USA), followed by concentrate collection from the inverted filter during 3 min at 1000x*g*.

*RNA Extraction***.** Concentrate (140-280 µL) was extracted using the QiaAmp Viral RNA MiniKit (Qiagen, USA) according to manufacturer's instructions, adapted to the larger volumes, and using 80 µL eluent volume. RNA extract was quantified immediately or within one week (storage at -80°C) using dPCR for SARS-CoV-2 N gene using both N1 and N2 markers. Separate RNA extract aliquots were stored at -80°C for less than three months for quantification of PMMoV genes. Samples were extracted once, and a negative extraction control using molecular grade water was run in parallel for every batch of extracted samples.

*Digital and Quantitative PCR***.** RNA extracts were used as a template (5 µl in 25 µl reaction) in digital droplet RT-PCR assays for SARS-CoV-2 N1 and N2 markers on the N gene as part of a triplex assay with RPP30 gene according to manufacturer's instructions (ddPCR Expert Design Assay: 2019-nCoV CDC ddPCR Triplex Probe Assay, dEXS28563542, Bio-Rad), and for a qRT-PCR assay for Pepper Mild Mottle Virus (PMMoV). Design and associated information on primers and probes are reported in Lu et al. for SARS-CoV-2 and Symonds et al. for PMMoV (52, 53). Samples were diluted 10-fold in a single step using molecular grade water before quantification in replicate wells. If the sample concentration was below the limit of quantification (LOQ), an undiluted sample was quantified (see Supplemental Information for LOQ). Positive controls consisting of 100 gc / reaction of synthetic SARS-CoV-2 RNA reference material (EURM-019, Joint Research Center) and negative controls consisting of RNAse/DNAse-free water were included in every thermocycler run. Mastermix, primer and probe sequences, thermocycling conditions, and dMIQE checklist (54) are provided in the Supplemental Information.

*Data Analysis and Quality Control***.** The limit of detection (LOD) and limit of quantification (LOQ) of the N1 and N2 markers were determined by processing 10 replicates of synthetic SARS-CoV-2 RNA reference material at target concentrations of 5, 8, 10, 25, 30, and 50 gc / reaction. LOD

was determined to be 8 copies / reaction (equivalent to 2560 copies / L wastewater), with greater than 95% likelihood of detection based on duplicate samples (55). LOQ was determined to be 25 gc / reaction (equivalent to 8000 gc / L wastewater), which was the lowest concentration with coefficient of variation less than 25% (55). When sample concentrations were below the LOQ, samples were processed without dilution. If undilute samples remained below LOQ, values were replaced with 16.5 gc/reaction, representing the mean of the LOQ and limit of detection (LOD, 8 gc/reaction, equivalent to 2560 gc/L wastewater).

Pepper Mild Mottle Virus (PMMoV), a plant virus that is found at high and constant concentrations in wastewater, was used as an internal process control to monitor fecal strength and detect anomalies in the collected sample or problems during concentration and extraction. in each sample (53). Samples with PMMoV loads ($\log_{10}$ gc / day) outside the mean plus or minus three times the standard deviation were excluded from further analysis. SARS-CoV-2 RNA concentrations were converted to loads by multiplying with the WWTP daily flow rate because normalization to flow was found to be superior to PMMoV based on correlation with clinical data (26).

PCR inhibition was tested by adding 800 genome copies / reaction of synthetic SARS-CoV-2 RNA reference material (EURM-019, Joint Research Center) to the mastermix in separate reactions. Samples were processed at the same dilution used for quantification of the N1 and N2 markers (see *Digital and Quantitative PCR*). Samples were considered inhibited if either the observed N1 or N2 concentration in the samples with synthetic SARS-CoV-2 RNA (spiked samples) was 80% or less than the sum of the concentration in the unspiked sample plus the concentration in the spiked, sample-free controls. Inhibited samples were removed from further analysis.

SARS-CoV-2 RNA quantification in primary sewage sludge (San Jose, CA, USA)

*Sample Collection and Preparation***.** From 15 November 2020 to 19 March 2021, 125 settled solids samples (approximately 50ml) were collected and processed daily from the primary settling tank at the San Jose wastewater treatment plant (San Jose, CA, USA) using methods adapted from Graham et al. and described in published protocols (15, 56–58).

Briefly, 24-hour composite samples were collected in clean plastic containers, immediately stored at 4°C, and transported to the lab for initial processing within 6 hrs of collection. The solids were dewatered by centrifugation at 24000xg for 30 minutes at 4°C. The supernatant was aspirated and discarded. A 0.5 - 1 g aliquot of the dewatered solids was dried at 110°C for 19-24 hrs to determine its dry weight. Dewatered solids were resuspended in Bovine Coronavirus (BCoV)-spiked DNA/RNA shield to a concentration of 75 mg/mL. This concentration of solids represented a concentration at which the inhibition of the SARS-CoV-2 assays was minimized based on experiments with solutions containing varying concentrations of solids (data not shown). BCoV was spiked as an external process control. To homogenize samples, 5-10 5/32” Stainless Steel Grinding Balls (OPS Diagnostics) were added to each sample before shaking with a Geno/Grinder 2010 (Spex SamplePrep). Samples were subsequently briefly centrifuged to remove air bubbles introduced during the homogenization process, and then vortexed to re-

mix the sample. Samples were either further processed immediately, or stored at 4°C for processing within 7 days.

*RNA Extraction***.** RNA was extracted from 300 µl of homogenized sample using the Chemagic™ Viral DNA/RNA 300 Kit H96 for the Perkin Elmer Chemagic 360 into 60 µl of eluent followed by PCR Inhibitor Removal with the Zymo OneStep-96 PCR Inhibitor Removal Kit (57). Each sample was extracted ten times. In addition, extraction negative and extraction positive controls, consisting of approximately 500 copies of SARS-CoV-2 genomic RNA (ATCC), were extracted using the same protocol as the homogenized samples in each batch of sample extraction.

*Digital PCR***.** RNA extracts were used as template in digital droplet RT-PCR assays for SARS-CoV-2 N, S, and ORF1a RNA gene targets in a triplex assay, and PMMoV and BCoV in a duplex assay. Undiluted extract was used for the SARS-CoV-2 assay template and a 1:100 dilution of the extract (2 µl into 198 µl molecular grade water) was used for the PMMoV and BCoV assay template. Primer and probe design, primer and probe sequences, mastermix, and thermocycling conditions are described in the Supplemental Information.
Each sample was run in 10 replicate wells, extraction negative controls were run in 7 wells, and extraction positive controls in 1 well. In addition, PCR positive controls for SARS-CoV-2 RNA were run in 1 well, and NTC were run in 7 wells. Results from replicate wells were merged for analysis.

*Data analysis and Quality Control***.** Concentrations of RNA targets were converted to concentrations per dry weight of solids in units of gene copies/g dry weight. PMMoV was also used to monitor fecal strength and virus recovery in the San Jose samples, using the same criteria as for the Zurich samples. BCoV was used to assess virus recovery, and samples were removed from further analysis if the amount recovered was less than 10% of the amount added.

Deconvolution by the Shedding Load Distribution

To relate the viral RNA loads or concentrations measured in wastewater to the number of new infections per day, we used information on the profile of SARS-CoV-2 RNA shedding into the wastewater by an infected individual in days after infection or symptom onset. In general, this profile contains information about both the magnitude and timing of viral RNA shedding: (i) the SLD $w(t)$ (sums to 1) describes the temporal dynamics of shedding, and (ii) a normalisation factor N describes the total amount of virus shed by an infected individual during the course of infection (in units of gc/infection). After shedding, downstream processes will further affect the total amount of viral RNA sampled per infected individual. We assume this does not affect the temporal dynamics, and can be summarised into a second normalisation factor M. In general, M will depend on the sewer system, wastewater treatment plant, choice of sample matrix and processing pipeline. The units of M differ depending on the way viral concentrations were measured. With these definitions, the measurement C_i of viral RNA in the wastewater on day i is related to past infections I_j on day j:

$$C_i = N \cdot M \sum_j w_{i-j} I_j \,,$$

i.e. the infections are convolved with the SLD.

For the main analysis, we deconvolved by a combination of the incubation period (the time from infection to symptom onset) and the gastrointestinal SLD from Benefield et al. for the time from symptom onset to shedding (24). Figure 3 from Benefield et al. (24) was digitised manually, and yielded a gamma distribution with mean 6.7 days and standard deviation 7.0 days (38). For the incubation period, we used the distribution of Linton et al.: a gamma distribution with mean 5.3 days and standard deviation 3.2 days (59). For additional comparisons (Fig. S2, S3), we exchanged the Benefield distribution for the SLD upon symptom onset reported by Han et al., gamma distributed with mean 4.7 days, standard deviation 1.7 days (23), or the symptom onset to death delay distribution from Linton et al., gamma distributed with mean 15 days, standard deviation 6.9 days (59).

Since the normalisation factors N and M are difficult to measure, and only influence R_{ww} point estimates when off by several orders of magnitude (Fig. S3), we made a simplifying assumption. We assumed the lowest measured RNA load (Zurich) or concentration (San Jose) represents the viral load or concentration from a single infection (N*M). For the Zurich wastewater data, this was 9.7*10^11 gc per infection, and for the San Jose sewage sludge measurements this was 2663.7 gc/g per infection.

Effective Reproductive Number Estimates

The effective reproductive number was estimated from SARS-CoV-2 RNA loads in wastewater or concentrations in sewage sludge using the pipeline developed in (2). In brief, we first transformed SARS-CoV-2 RNA measurements into a time series of infection incidence. To do so, we filled data gaps through linear interpolation, then smoothed and deconvolved the resulting time series with the SLD to obtain the infection incidence time series. Second, we used the package EpiEstim to estimate the effective reproductive number Re from this infection incidence (4, 60). The pipeline further accounts for noise in the observation process, by block bootstrapping the observations 50 times prior to smoothing and deconvolution.

The Zurich wastewater estimates were compared to R_{cc} based on cases reported for the catchment, obtained from the Health Department of Canton Zurich. To estimate R_{cc} specific to the catchment, we used the pipeline from (2), and deconvolved by a distribution specifying the delay from infection to case confirmation. This was parameterized as the sum of a gamma distributed incubation period with mean 5.3 days, standard deviation 3.2 days (59); and a gamma distributed delay from symptom onset to case confirmation with mean 2.8 days, standard deviation 3.0 days (estimated from line list data for canton Zurich, Sept 2020-Jan 2021). The reported R_{cc} values for confirmed cases, hospitalisations, and deaths at the cantonal level were taken from https://github.com/covid-19-Re/dailyRe-Data (based on (2)). For the Swiss data, “case confirmation” refers to the earliest recorded date of either a positive test or case reporting.

For comparison to the Californian wastewater data, we downloaded daily COVID-19 case incidence data for Santa Clara County from the California Health and Human Services Open

Data portal (https://data.chhs.ca.gov/dataset/covid-19-time-series-metrics-by-county-and-state). The wastewater from Santa Clara County (population of 1.7 million) is nearly all treated at the San Jose wastewater treatment plant (catchment population of 1.5 million). We estimated R_{cc} using the pipeline from (2), with the incubation period as before (59); and a gamma distributed symptom onset to case reporting delay distribution with a mean of 4.51 days and standard deviation of 3.16 days (estimated from line list data for Santa Clara County in December; based on personal correspondence with the California Department of Public Health COVID-19 modelling team). During the study period, the mean of this distribution varied between 3.31 and 5.24 days, and the standard deviation between 2.32 and 3.55 days. Negative numbers of cases reported (Dec 30) were set to 0. To estimate Re for the testing-adjusted cases, we extracted the daily number of positive tests / total number of tests, multiplied by the mean number of tests (8244.3). This time series was then used to estimate Re, similar to the confirmed cases (with the same delay distribution) (2). Technically, the tests are reported by testing date, rather than reporting date, so this constitutes a misspecification of the delay distribution. However, an analysis where the delay between symptom onset and testing was assumed 0 did not yield qualitatively different results (not shown). We additionally compared our estimates to the R_{cc} values for Santa Clara County from the California COVID assessment tool (https://calcat.covid19.ca.gov/cacovidmodels/).

Comparing Re traces

We assessed how well the Re estimates from SARS-CoV-2 concentrations in wastewater (R_{ww}) match those estimated from case report data (R_{cc}) using several measures. First, the average root mean squared error between both point estimates across the time series ("RMSE"):

$$\sqrt{\frac{1}{K}\sum_{j=1}^{K}\left(R_{ww,j} - R_{cc,j}\right)^2},$$

where *j* describes the date, and *K* the length of the time series. Second, the fraction of dates where the R_{ww} point estimate was within the confidence interval of the R_{cc} estimate ("coverage"). Third, the mean average percentage error between the time series ("MAPE"):

$$\frac{1}{K}\sum_{j=1}^{K}\left|\frac{R_{cc,j} - R_{ww,j}}{R_{cc,j}}\right|.$$

Scanning across shedding load distributions

To investigate optimal parameters for the SLD, we conducted two separate scans. In the first scan, we varied the parameters of the SLD from infection. In the second scan, we estimated the parameters of the SLD from symptom onset onwards. In the latter case, the delay sampled from the SLD was added to a second sampled delay corresponding to the incubation period (gamma distributed with mean 5.3 days and standard deviation of 3.2 days) (59). In both cases, we assumed the SLD was described by a gamma distribution, and varied the mean μ and standard deviation σ on a grid (μ $\in$ {0.5, 1.0, ..., 15} and $\sigma \in$ {0.5, 1.0, ..., 10}). The normalisation factor (N*M) was kept fixed to the location-specific value throughout. The R_{ww} for the wastewater data was estimated across 50 bootstrap samples and compared to the R_{cc} for the catchment.

Availability Statement

All code and case data for Zurich are publicly available through the Github repository https://github.com/JSHuisman/wastewaterRe. Wastewater measurements for Zurich are available at DOI: 10.25678/0003VC. Wastewater measurements from San Jose are available by request from ABB (aboehm@stanford.edu), and case data for Santa Clara County is available from the California Health and Human Services Open Data portal (https://data.chhs.ca.gov/dataset/covid-19-time-series-metrics-by-county-and-state).

Acknowledgements:

We thank members from the Bonhoeffer and Stadler groups for helpful discussions, Carola Bänziger, Claudia Scheckel (Oncobit AG, Switzerland), Bruno Mueller (Microsynth AG, Switzerland), and Sergey Yakushev (Microsynth AG, Switzerland) for assistance with and/or knowledge exchange on method development. We further thank the operators of the Zurich WWTPs for providing samples; the staff of the San Jose wastewater treatment plant including Payak Sarkar, Noel Enoki, and Amy Wong; the Health Department of Canton Zurich for catchment-specific case numbers; and the California Department of Public Health Covid-19 modelling team for input on the Re estimates and symptom onset to case confirmation delay distribution for the state of California. XFC, TS, CO, TRJ and TK acknowledge funding from the Swiss National Science foundation (Special Call on Coronaviruses; 31CA30_196267 and 31CA30_196538). CO, TRJ and TK further acknowledge discretionary funding from Eawag and EPFL. XFC was a fellow of the European Union's Horizon 2020 research and innovation programme under the Marie Skłodowska–Curie Grant Agreement No. 754462. The San Jose wastewater data acquisition and curation was funded by the CDC-Foundation.

Author contributions:

JSH, TK, CO, TS, TRJ conceived the study; JSH developed the analytical framework, designed and performed computational analyses; JS, AS, TS contributed to the analytical methods; LC, XFC, PG, AKu, ES, ABB, BH, AKn, AT, KRW, MKW, TK, CO, TRJ developed experimental protocols and performed wastewater sampling; XFC, ABB, KRW, TK, CO, TS, TRJ supervised the study and secured funding; JSH, TK, TRJ wrote the original draft; all authors reviewed and approved the final manuscript.

References:

1. K. M. Gostic, *et al.*, Practical considerations for measuring the effective reproductive number, R t. *PLoS Comput. Biol.* **16**, e1008409 (2020).

2. J. S. Huisman, *et al.*, Estimation and worldwide monitoring of the effective reproductive number of SARS-CoV-2. *medrxiv* (2020).

3. J. Wallinga, P. Teunis, Different epidemic curves for severe acute respiratory syndrome reveal similar impacts of control measures. *Am. J. Epidemiol.* **160**, 509–516 (2004).

4. A. Cori, N. M. Ferguson, C. Fraser, S. Cauchemez, A new framework and software to estimate time-varying reproduction numbers during epidemics. *Am. J. Epidemiol.* **178**, 1505–1512 (2013).

5. J. M. Brauner, *et al.*, Inferring the effectiveness of government interventions against COVID-19. *Science* **371** (2021).

6. Der Schweizerische Bundesrat, "Verordnung über Massnahmen in der besonderen Lage zur Bekämpfung der Covid-19-Epidemie" (2020).

7. R. Anderson, *et al.*, "Reproduction number (R) and growth rate (r) of the COVID-19 epidemic in the UK: methods of estimation, data sources, causes of heterogeneity, and use as a guide in policy formulation" (The Royal Society, 2020).

8. T. Yabe, *et al.*, Non-compulsory measures sufficiently reduced human mobility in Tokyo during the COVID-19 epidemic. *Sci. Rep.* **10**, 18053 (2020).

9. A. Pan, *et al.*, Association of Public Health Interventions With the Epidemiology of the COVID-19 Outbreak in Wuhan, China. *JAMA* **323**, 1915–1923 (2020).

10. S. Flaxman, *et al.*, Estimating the effects of non-pharmaceutical interventions on COVID-19 in Europe. *Nature* **584**, 257–261 (2020).

11. K. Soltesz, *et al.*, The effect of interventions on COVID-19. *Nature* **588**, E26–E28 (2020).

12. L. M. Rossen, A. M. Branum, F. B. Ahmad, P. Sutton, R. N. Anderson, Excess Deaths Associated with COVID-19, by Age and Race and Ethnicity — United States, January 26–October 3, 2020. *MMWR. Morbidity and Mortality Weekly Report* **69**, 1522–1527 (2020).

13. J. Peccia, *et al.*, Measurement of SARS-CoV-2 RNA in wastewater tracks community infection dynamics. *Nat. Biotechnol.* **38**, 1164–1167 (2020).

14. S. Karthikeyan, *et al.*, High-Throughput Wastewater SARS-CoV-2 Detection Enables Forecasting of Community Infection Dynamics in San Diego County. *mSystems* **6** (2021).

15. K. E. Graham, *et al.*, SARS-CoV-2 RNA in Wastewater Settled Solids Is Associated with COVID-19 Cases in a Large Urban Sewershed. *Environ. Sci. Technol.* **55**, 488–498 (2021).

16. G. Medema, L. Heijnen, G. Elsinga, R. Italiaander, A. Brouwer, Presence of SARS-Coronavirus-2 RNA in Sewage and Correlation with Reported COVID-19 Prevalence in the Early Stage of the Epidemic in The Netherlands. *Environ. Sci. Technol. Lett.* **7**, 511–516

(2020).

17. S. Agrawal, L. Orschler, S. Lackner, Long-term monitoring of SARS-CoV-2 RNA in wastewater of the Frankfurt metropolitan area in Southern Germany. *Sci. Rep.* **11**, 5372 (2021).

18. S. Arora, *et al.*, Sewage surveillance for the presence of SARS-CoV-2 genome as a useful wastewater based epidemiology (WBE) tracking tool in India. *Water Sci. Technol.* **82**, 2823–2836 (2020).

19. E. Haramoto, B. Malla, O. Thakali, M. Kitajima, First environmental surveillance for the presence of SARS-CoV-2 RNA in wastewater and river water in Japan. *Sci. Total Environ.* **737**, 140405 (2020).

20. E. H. Kaplan, *et al.*, Aligning SARS-CoV-2 indicators via an epidemic model: application to hospital admissions and RNA detection in sewage sludge. *Health Care Manag. Sci.* (2020) https:/doi.org/10.1007/s10729-020-09525-1.

21. C. S. McMahan, *et al.*, COVID-19 Wastewater Epidemiology: A Model to Estimate Infected Populations. *MedRxiv* (2020).

22. R. Wölfel, *et al.*, Virological assessment of hospitalized patients with COVID-2019. *Nature* **581**, 465–469 (2020).

23. M. S. Han, *et al.*, Viral RNA Load in Mildly Symptomatic and Asymptomatic Children with COVID-19, Seoul, South Korea. *Emerg. Infect. Dis.* **26**, 2497–2499 (2020).

24. A. E. Benefield, *et al.*, SARS-CoV-2 viral load peaks prior to symptom onset: a systematic review and individual-pooled analysis of coronavirus viral load from 66 studies. *medRxiv* (2020).

25. Q. Li, *et al.*, Early Transmission Dynamics in Wuhan, China, of Novel Coronavirus–Infected Pneumonia. *N. Engl. J. Med.* **382**, 1199–1207 (2020).

26. S. Feng, *et al.*, Evaluation of sampling frequency and normalization of SARS-CoV-2 wastewater concentrations for capturing COVID-19 burdens in the community. *medRxiv* (2021).

27. M. Kitajima, *et al.*, SARS-CoV-2 in wastewater: State of the knowledge and research needs. *Sci. Total Environ.* **739**, 139076 (2020).

28. M. Cevik, *et al.*, SARS-CoV-2, SARS-CoV, and MERS-CoV viral load dynamics, duration of viral shedding, and infectiousness: a systematic review and meta-analysis. *Lancet Microbe* **2**, e13–e22 (2021).

29. S. Zheng, *et al.*, Viral load dynamics and disease severity in patients infected with SARS-CoV-2 in Zhejiang province, China, January-March 2020: retrospective cohort study. *BMJ* **369**, m1443 (2020).

30. K. A. Walsh, *et al.*, SARS-CoV-2 detection, viral load and infectivity over the course of an infection. *J. Infect.* **81**, 357–371 (2020).

31. T. Hoffmann, J. Alsing, Faecal shedding models for SARS-CoV-2 RNA amongst

hospitalised patients and implications for wastewater-based epidemiology. *medRxiv* (2021).

32. Y. Liu, *et al.*, Viral dynamics in mild and severe cases of COVID-19. *Lancet Infect. Dis.* **20**, 656–657 (2020).

33. C. Zhou, *et al.*, Impact of age on duration of viral RNA shedding in patients with COVID-19. *Aging* **12**, 22399–22404 (2020).

34. K. V. Parag, Improved estimation of time-varying reproduction numbers at low case incidence and between epidemic waves. *medRxiv* (2020).

35. S. Abbott, *et al.*, Estimating the time-varying reproduction number of SARS-CoV-2 using national and subnational case counts. *Wellcome Open Research* **5**, 112 (2020).

36. S. Stringhini, *et al.*, Seroprevalence of anti-SARS-CoV-2 IgG antibodies in Geneva, Switzerland (SEROCoV-POP): a population-based study. *Lancet* **396**, 313–319 (2020).

37. S. Stringhini, *et al.*, Seroprevalence of anti-SARS-CoV-2 antibodies after the second pandemic peak. *The Lancet Infectious Diseases* (2021) https:/doi.org/10.1016/s1473-3099(21)00054-2.

38. X. Fernandez-Cassi, *et al.*, Wastewater monitoring outperforms case numbers as a tool to track COVID-19 incidence dynamics when test positivity rates are high https:/doi.org/10.1101/2021.03.25.21254344.

39. K. W. Heaton, *et al.*, Defecation frequency and timing, and stool form in the general population: a prospective study. *Gut* **33**, 818–824 (1992).

40. K. V. Thomas, A. Amador, J. A. Baz-Lomba, M. Reid, Use of Mobile Device Data To Better Estimate Dynamic Population Size for Wastewater-Based Epidemiology. *Environ. Sci. Technol.* **51**, 11363–11370 (2017).

41. R. S. Kantor, K. L. Nelson, H. D. Greenwald, L. C. Kennedy, Challenges in Measuring the Recovery of SARS-CoV-2 from Wastewater. *Environ. Sci. Technol.* **55**, 3514–3519 (2021).

42. L. C. de Oliveira, *et al.*, Viability of SARS-CoV-2 in river water and wastewater at different temperatures and solids content. *Water Res.* **195**, 117002 (2021).

43. A. Bivins, *et al.*, Persistence of SARS-CoV-2 in Water and Wastewater. *Environ. Sci. Technol. Lett.* **7**, 937–942 (2020).

44. A.-M. Hokajärvi, *et al.*, The detection and stability of the SARS-CoV-2 RNA biomarkers in wastewater influent in Helsinki, Finland. *Sci. Total Environ.* **770**, 145274 (2021).

45. D. Gerrity, K. Papp, M. Stoker, A. Sims, W. Frehner, Early-pandemic wastewater surveillance of SARS-CoV-2 in Southern Nevada: Methodology, occurrence, and incidence/prevalence considerations. *Water Res X* **10**, 100086 (2021).

46. K. Jahn, *et al.*, Detection of SARS-CoV-2 variants in Switzerland by genomic analysis of wastewater samples. *medRxiv* (2021).

47. A. Crits-Christoph, *et al.*, Genome Sequencing of Sewage Detects Regionally Prevalent SARS-CoV-2 Variants. *MBio* **12** (2021).

48. J. Martin, *et al.*, Tracking SARS-CoV-2 in Sewage: Evidence of Changes in Virus Variant Predominance during COVID-19 Pandemic. *Viruses* **12** (2020).

49. N. E. Brinkman, G. S. Fout, S. P. Keely, Retrospective Surveillance of Wastewater To Examine Seasonal Dynamics of Enterovirus Infections. *mSphere* **2** (2017).

50. S. Kazama, *et al.*, Temporal dynamics of norovirus determined through monitoring of municipal wastewater by pyrosequencing and virological surveillance of gastroenteritis cases. *Water Res.* **92**, 244–253 (2016).

51. C. McCall, H. Wu, B. Miyani, I. Xagoraraki, Identification of multiple potential viral diseases in a large urban center using wastewater surveillance. *Water Res.* **184**, 116160 (2020).

52. X. Lu, *et al.*, US CDC Real-Time Reverse Transcription PCR Panel for Detection of Severe Acute Respiratory Syndrome Coronavirus 2. *Emerg. Infect. Dis.* **26** (2020).

53. Symonds EM, Nguyen KH, Harwood VJ, Breitbart M, Pepper mild mottle virus: A plant pathogen with a greater purpose in (waste)water treatment development and public health management. *Water Res.* **144**, 1–12 (2018).

54. dMIQE Group, J. F. Huggett, The Digital MIQE Guidelines Update: Minimum Information for Publication of Quantitative Digital PCR Experiments for 2020. *Clin. Chem.* **66**, 1012–1029 (2020).

55. K. Zhu, B. Suttner, A. Pickering, K. T. Konstantinidis, J. Brown, A novel droplet digital PCR human mtDNA assay for fecal source tracking. *Water Res.* **183**, 116085 (2020).

56. A. Topol, M. Wolfe, B. White, K. Wigginton, A. Boehm, High Throughput pre-analytical processing of wastewater settled solids for SARS-CoV-2 RNA analyses v1 (protocols.io.btyqnpvw). *protocols.io* (2021) https:/doi.org/10.17504/protocols.io.btyqnpvw.

57. A. Topol, M. Wolfe, K. Wigginton, B. White, A. Boehm, High Throughput RNA Extraction and PCR Inhibitor Removal of Settled Solids for Wastewater Surveillance of SARS-CoV-2 RNA v1 (protocols.io.btyrnpv6). *protocols.io* (2021) https:/doi.org/10.17504/protocols.io.btyrnpv6.

58. A. Topol, M. Wolfe, B. White, K. Wigginton, A. Boehm, High Throughput SARS-COV-2, PMMOV, and BCoV quantification in settled solids using digital RT-PCR v1 (protocols.io.btywnpxe). *protocols.io* (2021) https:/doi.org/10.17504/protocols.io.btywnpxe.

59. N. M. Linton, *et al.*, Incubation period and other epidemiological characteristics of 2019 novel Coronavirus infections with right truncation: A statistical analysis of publicly available case data. *J. Clin. Med. Res.* **9**, 538 (2020).

60. A. Cori, *et al.*, EpiEstim: estimate time varying reproduction numbers from epidemic curves. *R package version*, 2–2 (2019).

61. E. Haramoto, *et al.*, Occurrence of pepper mild mottle virus in drinking water sources in Japan. *Appl. Environ. Microbiol.* **79**, 7413–7418 (2013).

62. T. Zhang, *et al.*, RNA Viral Community in Human Feces: Prevalence of Plant Pathogenic Viruses. *PLoS Biol.* **4**, e3 (2005).

Supplemental Material:

Fig. S1: The estimated infection incidence (A) and R_e (B) in San Jose. These results are the same as Fig. 2C, D; except we added estimates of the testing-adjusted cases. The testing-adjusted cases describe the number of positive tests / total number of tests per day, normalised by the mean number of tests per day in Santa Clara during the study period. (A) The estimated time series of infection incidence from case reports (top), testing-adjusted cases (middle) and normalised RNA concentrations (bottom). The gene copies per gram dry weight were normalised by assuming the lowest measured value represents the viral concentration in sewage resulting from a single infection (M*N=2663.7 gc/g per infection; see Methods). The bars indicate the mean ± standard deviation across 50 bootstrap replicates. (B) The estimated R_{ww} compared to R_{cc} from confirmed cases and testing-adjusted cases. The coloured line indicates the point estimate on the original data, and the ribbons the 95% confidence interval across 50 bootstrap replicates.

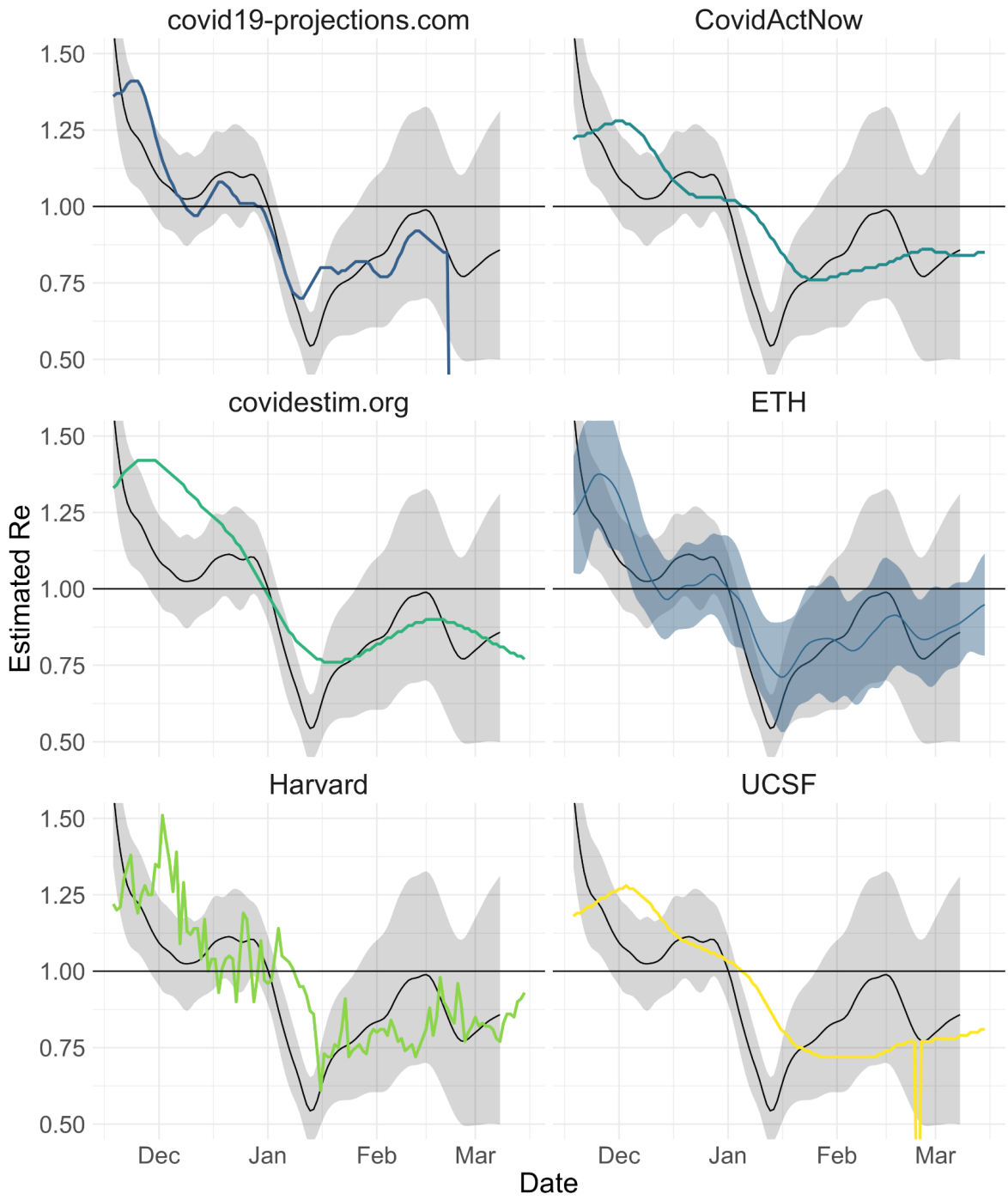

Fig. S2: The estimated R_{ww} in San Jose (black, N gene) compared to different R_{cc} estimates for Santa Clara county from the CalCat website (https://calcat.covid19.ca.gov/cacovidmodels/**).** "ETH" refers to the pipeline of Huisman et al. (2) applied to the daily confirmed case data from Santa Clara county, i.e. the same comparison as shown in Fig 2D. We excluded the SEIR model based estimates included on the CalCat website (since these performed visibly worse than the other methods).

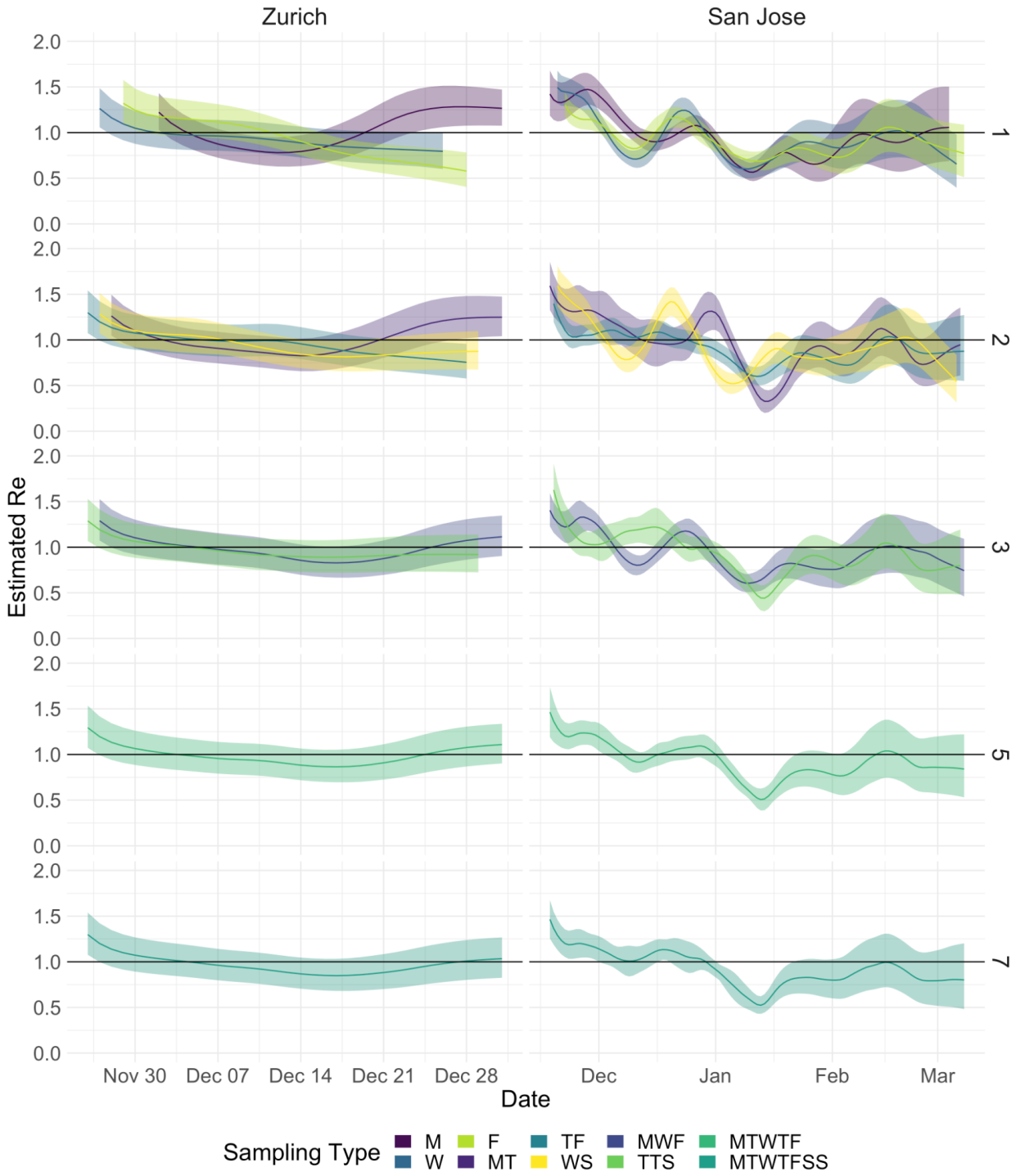

Fig. S3: The effect of sampling frequency on the R_{ww} estimates in Zurich and San Jose. The row label indicates the number of samples taken per week (1, 2, 3, 5, 7), while the colours indicate the sampling schedule: MTWTFSS corresponds to daily sampling, MTWTF sampling during the working week, MWF Mon-Wed-Fri, TTS Tue-Thu-Sat, MT Mon-Thu, TF Tue-Fri, WS Wed-Sat, M Monday, W Wednesday, F Friday.

Table S1: The match between the daily and further subsampled R_{ww} traces for Zurich. The data stems from measurements of the N1 marker for Zurich between 2020-11-22 and 2021-01-11. All traces are compared to the daily sampling; MTWTF corresponds to sampling during the working week, MWF Mon-Wed-Fri, TTS Tue-Thu-Sat, MT Mon-Thu, TF Tue-Fri, WS Wed-Sat, M Monday, W Wednesday, F Friday.

	MTWTF	MWF	TTS	MT	TF	WS	M	W	F
RMSE	0.03	0.04	0.03	0.12	0.09	0.06	0.17	0.06	0.18
Coverage	1.00	0.97	0.94	0.78	0.83	0.92	0.53	0.83	0.61
MAPE	0.02	0.03	0.02	0.09	0.07	0.05	0.12	0.04	0.17

Table S2: The match between the daily and further subsampled R_{ww} traces for San Jose. The data stems from the S gene measurements for San Jose. All traces are compared to the daily sampling; MTWTF corresponds to sampling during the working week, MWF Mon-Wed-Fri, TTS Tue-Thu-Sat, MT Mon-Thu, TF Tue-Fri, WS Wed-Sat, M Monday, W Wednesday, F Friday.

	MTWTF	MWF	TTS	MT	TF	WS	M	W	F
RMSE	0.05	0.09	0.08	0.15	0.06	0.16	0.13	0.13	0.08
Coverage	0.95	0.88	0.91	0.83	0.93	0.60	0.76	0.68	0.84
MAPE	0.05	0.08	0.07	0.15	0.06	0.14	0.11	0.11	0.07

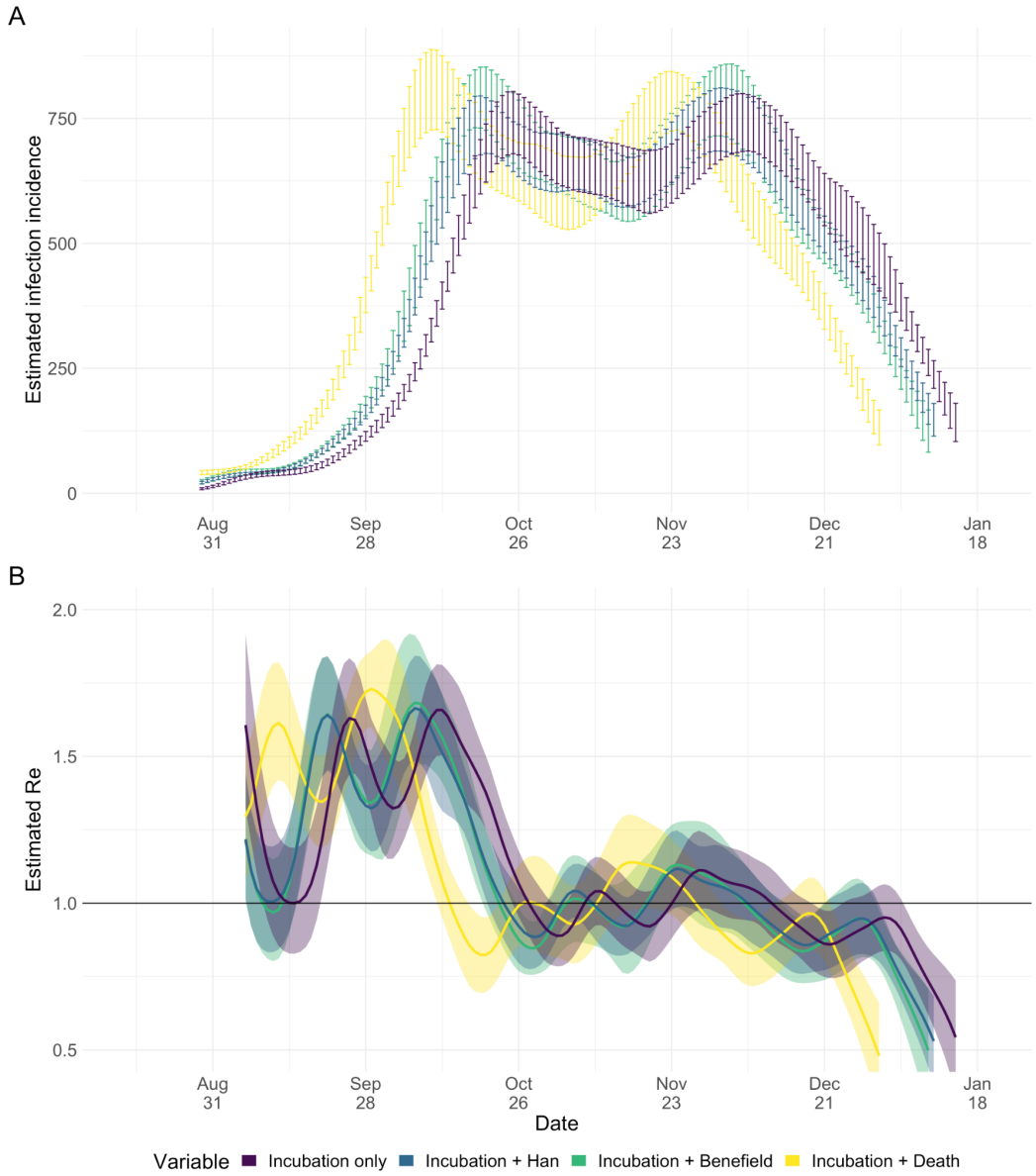

Fig. S4: The impact of the shedding load distribution on (A) the inferred infection incidence and (B) R_{ww} estimation from the Zurich wastewater data. The results are compared for four SLDs (see Methods): the Benefield SLD upon symptom onset (Incubation + Benefield) (24), the Han SLD upon symptom onset (Incubation + Han) (23, 24), shedding only on the day of symptom onset (Incubation only), shedding only on the day of death (Incubation + Death) (59).

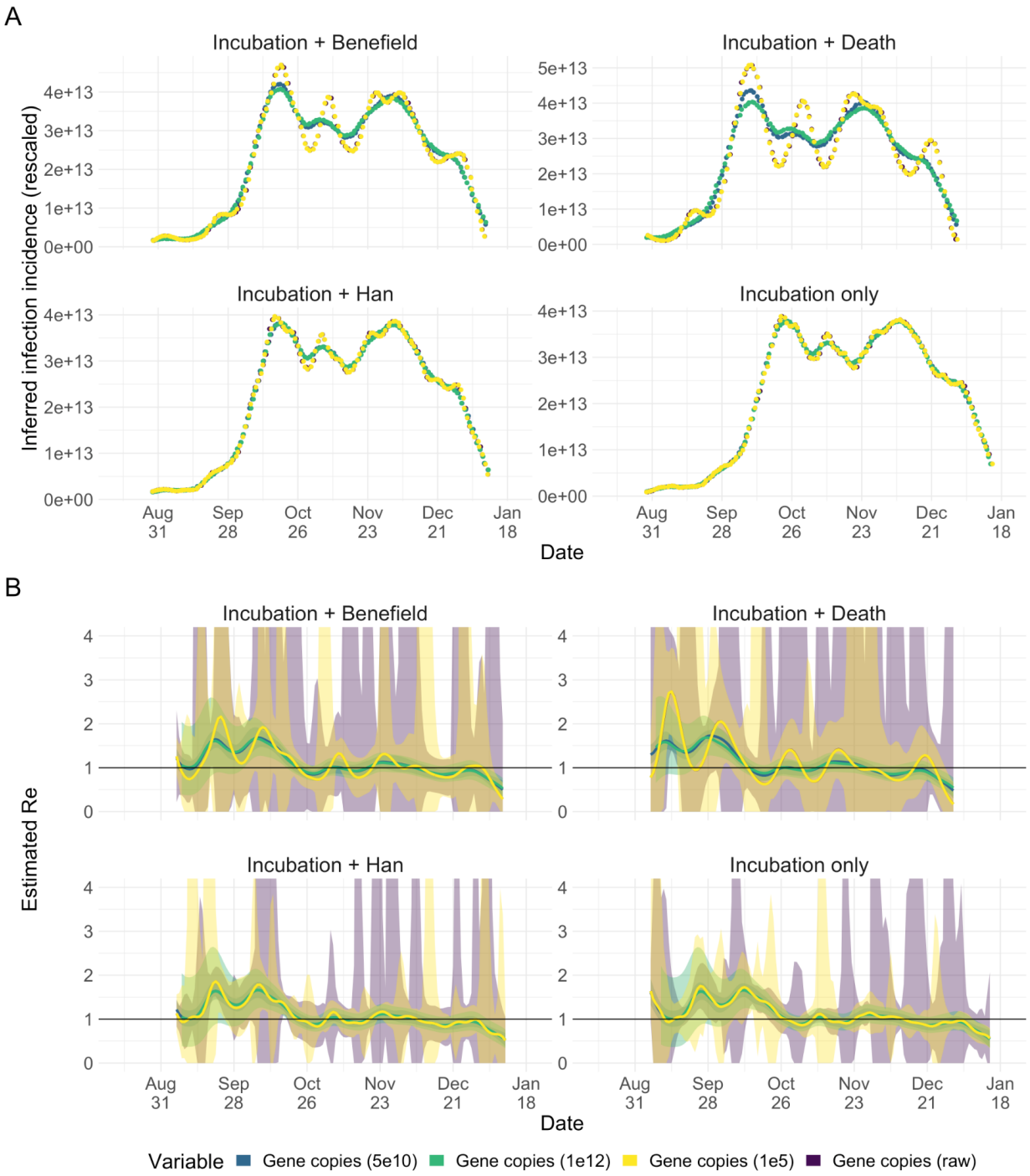

Fig. S5: The effect of data normalisation on the estimated R_{ww} in Zurich. We calculated R_{ww} from the measured N1 marker indicating the N gene copy loads, normalised in four different ways: by 1x10^12 gc per infection (the order of magnitude of the lowest measured concentration), by 5x10^10gc per infection (roughly rescaled to case incidence), by 1x10^5 gc per infection (to cover the space of possible orders of magnitude), no normalisation. **(A)** After normalisation the measurements were deconvolved, and rescaled back to the original magnitude (multiplied by the normalisation factor) to illustrate differences in the inferred infection

incidence. **(B)** The resulting R_{ww} estimates differ both in the mean (due to the deconvolution illustrated in A) and width of the uncertainty interval. The results are compared for four SLDs (panels; see Methods): the Benefield SLD upon symptom onset (Incubation + Benefield) (24), the Han SLD upon symptom onset (Incubation + Han) (23, 24), shedding only on the day of symptom onset (Incubation only), shedding only on the day of death (Incubation + Death) (59).

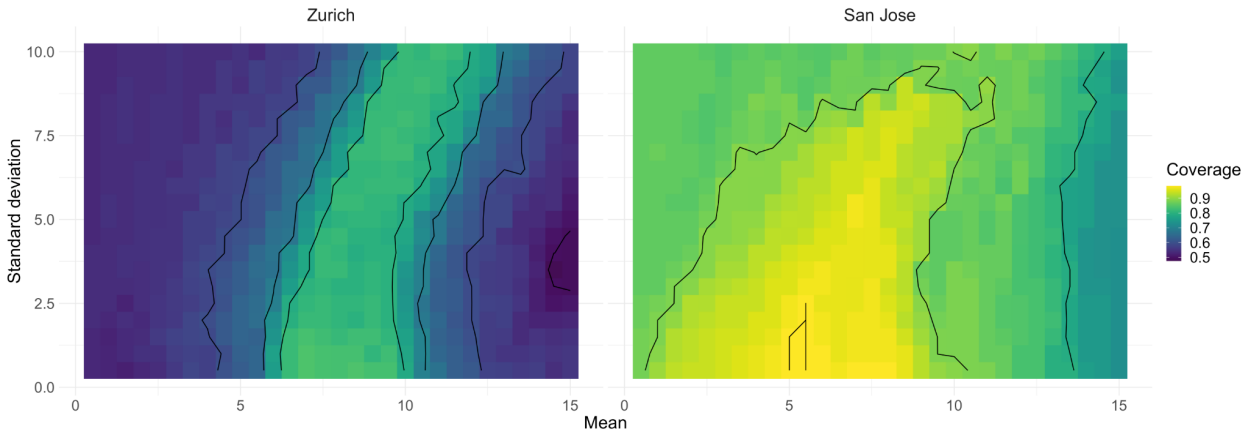

Fig. S6: Coverage between R_{cc} and R_{ww} for different shedding load distributions. We scanned across different (mean, standard deviation) parameter pairs for the SLD from time since infection. For the city of Zurich, the R_{ww} from N1 loads in wastewater was compared to that of confirmed cases in the catchment. For San Jose, we compared S gene concentrations to confirmed cases in Santa Clara County. The contour lines show SLD parameter pairs with equal coverage, in steps of 10% of the optimum value.

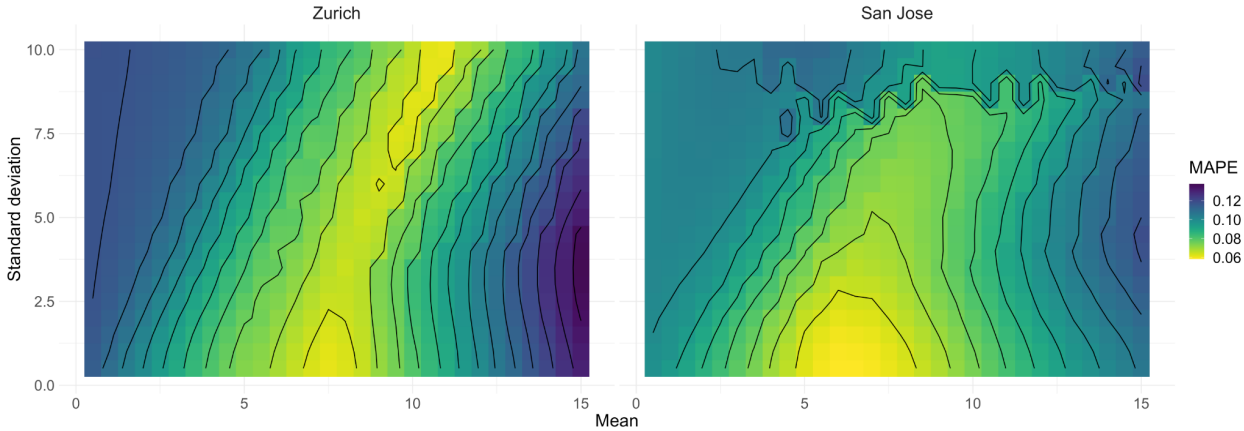

Fig. S7: MAPE between R_{cc} and R_{ww} for different shedding load distributions. We scanned across different (mean, standard deviation) parameter pairs for the SLD from time since infection. For the city of Zurich, the R_{ww} from N1 loads in wastewater was compared to that of confirmed cases in the catchment. For San Jose, we compared S gene concentrations to confirmed cases in Santa Clara County. The contour lines show SLD parameter pairs with equal MAPE, in steps of 10% of the optimum value.

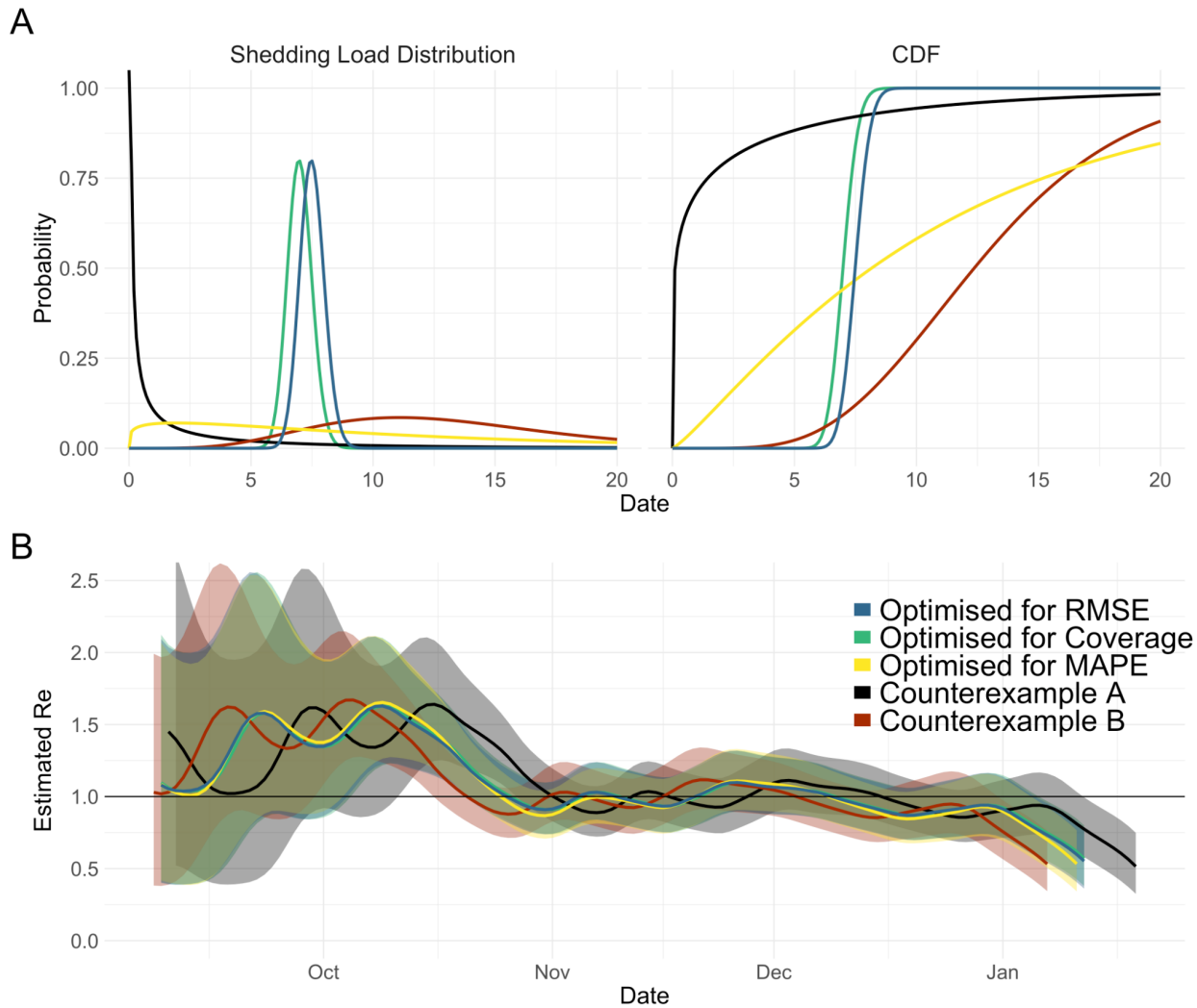

Fig. S8: The optimal shedding load distributions for Zurich and two counterexamples. Counterexample A has a mean of 2 days and standard deviation of 5 days; Counterexample B a mean of 13 days, and a standard deviation of 5 days. **(A)** The SLDs and their associated cumulative distribution functions. Although the SLDs differ when optimised for RMSE, Coverage, or MAPE, the median (i.e. the time after which they reach half their overall probability mass) is very comparable. **(B)** The resulting R_{ww} estimates for Zurich are highly similar for RMSE, Coverage, and MAPE based optimal SLDs; but differ substantially for the two counterexamples.

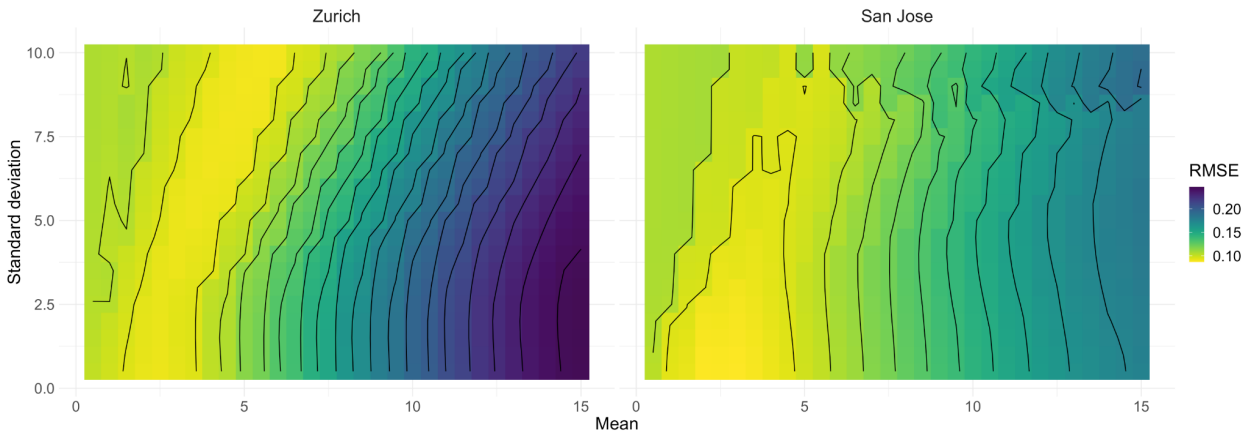

Fig. S9: RMSE between R_{cc} and R_{ww} for different shedding load distributions from symptom onset. We scanned across different (mean, standard deviation) parameter pairs for the SLD from time since symptom onset. For the city of Zurich, the Re from N1 loads in wastewater was compared to that of confirmed cases in the catchment. For San Jose, we compared S gene concentrations to confirmed cases in Santa Clara County. The incubation period is assumed gamma distributed with mean 5.3, and standard deviation 3.2. The contour lines show SLD parameter pairs with equal RMSE, in steps of 10% of the optimum value.

Table S3: Parameters of the optimal shedding distribution from symptom onset. We scanned across different (mean, standard deviation) parameter pairs for the SLD from time since symptom onset. For the city of Zurich, the R_{ww} from N1 loads in wastewater was compared to that of confirmed cases in the catchment. For San Jose, we compared S gene concentrations to confirmed cases in Santa Clara County. For all RMSE values of the scan see Fig. S9. All parameters are in units of days.

Comparison	Optimal pair (mean; sd)	Mean within 10% of the optimum	SD within 10% of the optimum
RMSE (Zurich)	(5.5; 10)	[1.5, 7]	[0.5, 10]
Coverage (Zurich)	(3.5; 5)	[1.5, 8]	[0.5, 10]
MAPE (Zurich)	(5.5; 10)	[2, 6]	[0.5, 10]
RMSE (San Jose)	(3; 0.5)	[1, 5]	[0.5, 9]
Coverage (San Jose)	(0.5; 0.5)	[0.5, 6]	[0.5, 10]
MAPE (San Jose)	(1; 0.5)	[0.5, 3]	[0.5, 10]

Table S4: Primer and Probes

Site	Target	Primer/Probe	Sequence
Zurich	N1	Forward	GACCCCAAAATCAGCGAAAT
		Reverse	GACCCCAAAATCAGCGAAAT
		Probe	ACCCCGCATTACGTTTGGTGGACC (5’ FAM/ZEN/3’ IBFQ)
	N2	Forward	TTACAAACATTGGCCGCAAA
		Reverse	GCGCGACATTCCGAAGAA
		Probe	ACAATTTGCCCCCAGCGCTTCAG (5’ FAM/HEX/ZEN/ 3’ IBFQ)
	PMMoV	Forward	GAGTGGTTTGACCTTAACGTTTGA
		Reverse	TTGTCGGTTGCAATGCAAGT
		Probe	CCTACCGAAGCAAATG (5’ FAM/3’ MGB)
San Jose	N Gene	Forward	CATTACGTTTGGTGGACCCT
		Reverse	CCTTGCCATGTTGAGTGAGA
		Probe	CGCGATCAAAACAACGTCGG (5’ FAM/ZEN/3’ IBFQ)
	S Gene	Forward	CAGACTAATTCTCCTCGGCG
		Reverse	TGCACCAAGTGACATAGTGT
		Probe	AGCTAGTCAATCCATCATTGCCT (5’ HEX/ZEN/3’ IBFQ)
	ORF1a	Forward	CAGAACTGGAACCACCTTGT
		Reverse	TACAGTTGAATTGGCAGGCA
		Probe	TGCCACAGTACGTCTACAAGC (5’ FAM or HEX/ZEN/3’ IBFQ)

PMMoV	Forward	GAGTGGTTTGACCTTAACGTTTGA
	Reverse	TTGTCGGTTGCAATGCAAGT
	Probe	CCTACCGAAGCAAATG (5’ HEX/ZEN/3’ IBFQ)
BCoV	Forward	CTGGAAGTTGGTGGAGTT
	Reverse	ATTATCGGCCTAACATACATC
	Probe	CCTTCATATCTATACACATCAAGTTGTT (5’ FAM/ZEN/3’ IBFQ)

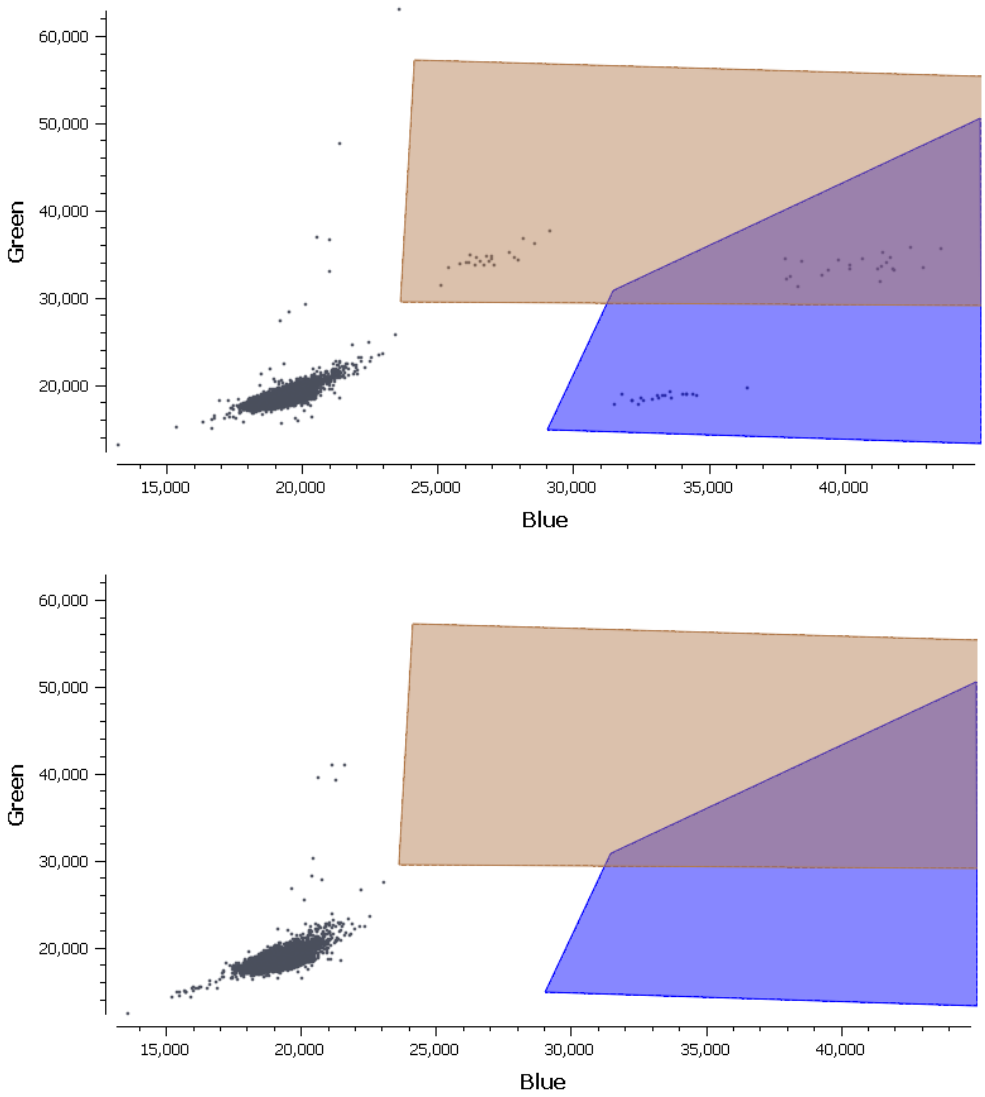

Fig. S10: Fluorescence plots from the Stilla Naica Crystal Droplet PCR used for the wastewater samples from Zurich collected after 23 September 2020 from positive (top) and negative (bottom) experimental results. Droplets positive for N1 (blue) and N2 (brown) and both N1 and N2 (purple). RPP30 markers, detectable as elevated fluorescence in Green channel, are included in the commercial assay used, but are not further analyzed.

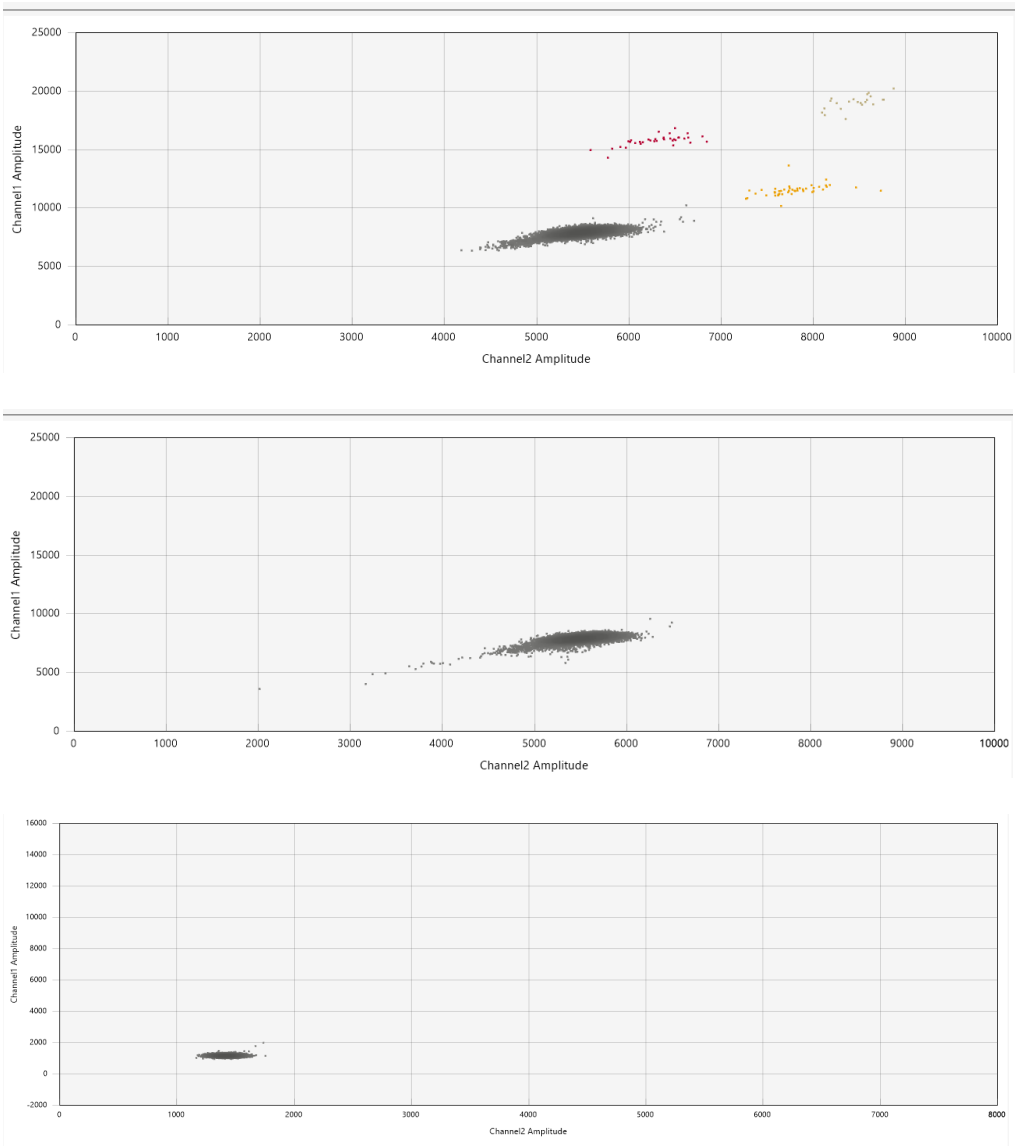

Fig. S11: Fluorescence plots from the Bio-Rad QX200 used for the wastewater samples. Samples from Zurich collected from 03-20 September 2020 are shown in positive (top) and negative (middle) experimental results. Droplets positive for N1 (red) and N2 (yellow) and both N1 and N2 (brown) markers. Negative (bottom) experimental results are also shown for San Jose Corresponding positive experimental results are provided in the reference of the associated protocol (58).

ITEM TO CHECK	PROVIDED	COMMENT
	Y/N	
1. SPECIMEN		
Detailed description of specimen type and numbers	Y	Methods of Main Text
Sampling procedure (including time to storage)	Y	Methods of Main Text
Sample aliquotation, storage conditions and duration	Y	Methods of Main Text
2. NUCLEIC ACID EXTRACTION		
Description of extraction method including amount of sample	Y	Methods of Main Text
Volume of solvent used to elute/resuspend extract	Y	Methods of Main Text
Number of extraction replicates	Y	Methods of Main Text
Extraction blanks included?	Y	Methods of Main Text
3. NUCLEIC ACID ASSESSMENT AND STORAGE		
Method to evaluate quality of nucleic acids	N	Not Done
Method to evaluate quantity of nucleic acids (including molecular	N	Not Done
Storage conditions: temperature, concentration, duration, buffer, aliquots	Y	Methods of Main Text
Clear description of dilution steps used to prepare working DNA solution	Y	Methods of Main Text
4. NUCLEIC ACID MODIFICATION		
Template modification (digestion, sonication, pre-amplification,	N	NA
Details of repurification following modification if performed	Y	No Repurification for Zurich Samples, Zymo Column for San Jose Samples Described in Methods of Main Text
5. REVERSE TRANSCRIPTION		
cDNA priming method and concentration	N	NA
One or two step protocol (include reaction details for two step)	Y	Methods of Main Text
Amount of RNA added per reaction	Y	Methods of Main Text
Detailed reaction components and conditions	Y	Supplemental Information
Estimated copies measured with and without addition of RT*	N	Not Done
Manufacturer of reagents used with catalogue and lot numbers	N	Reagents, Manufacturers, and Catalogue Numbers Reported in Supplemental Material. Lot Numbers are Not Reported
Storage of cDNA: temperature, concentration, duration, buffer and	Y	NA
6. dPCR OLIGONUCLEOTIDES DESIGN AND TARGET INFORMATION		
Sequence accession number or official gene symbol	Y	Published Reference (Zurich) or Supplemental (San Jose)
Method (software) used for design and *in silico* verification	Y	Published Reference (Zurich) or Supplemental (San Jose)
Location of amplicon	Y	Published Reference (Zurich) or Supplemental (San Jose)
Amplicon length	Y	Published Reference (Zurich) or Supplemental (San Jose)
Primer and probe sequences (or amplicon context sequence)**	Y	Supplemental Information
Location and identity of any modifications	Y	NA
Manufacturer of oligonucleotides	Y	Supplemental Information
7. dPCR PROTOCOL		
Manufacturer of dPCR instrument and instrument model	Y	Supplemental Information
Buffer/kit manufacturer with catalogue and lot number	Y	Supplemental Information
Primer and probe concentration	Y	Supplemental Information
Pre-reaction volume and composition (incl. amount of template	Y	Supplemental Information
Template treatment (initial heating or chemical denaturation)	N	NA
Polymerase identity and concentration, Mg++ and dNTP concentrations***	N	Included in Kit Manuals
Complete thermocycling parameters	Y	Supplemental Information
8. ASSAY VALIDATION		
Details of optimisation performed	N	Commercial Kit, Followed Manufacturer's Instructions
Analytical specificity (vs. related sequences) and limit of blank (LOB)	N	Not done (Zurich) or Supplemental (San Jose)
Analytical sensitivity/LoD and how this was evaluated	Y	Methods of Main Text
Testing for inhibitors (from biological matrix/extraction)	Y	Methods of Main Text
9. DATA ANALYSIS		
Description of dPCR experimental design	Y	Methods of Main Text
Comprehensive details negative and positive of controls (whether a	Y	Methods of Main Text
Partition classification method (thresholding)	Y	Supplemental Information
Examples of positive and negative experimental results (including	Y	Supplemental Information
Description of technical replication	Y	Methods of Main Text
Repeatability (intra-experiment variation)	Y	Supplemental Information
Reproducibility (inter-experiment/user/lab etc. variation)	N	Assays were only completed within one laboratory
Number of partitions measured (average and standard deviation)	Y	Supplemental Information
Partition volume	Y	Reported by Manufacturer
Copies per partition (λ or equivalent) (average and standard deviation)	Y	Supplemental Information
dPCR analysis program (source, version)	Y	Methods of Main Text
Description of normalisation method	N	NA
Statistical methods used for analysis	Y	Methods of Main Text
Data transparency	raw data available on request:	Data Availability Statement Includes Resources for Zurich Measurements, Contact Information for San Jose Measurements

Figure S12: dMIQE Checklist (54) **for RT-dPCR assays targeting SARS-CoV-2 gene markers N1 and N2 (Zurich Site) and S, N, and Orf1a (San Jose Site).** Checklist is not included for other RT-qPCR (PMMoV, Zurich Site) or RT-dPCR (BCoV, PMMoV, San Jose) Assays.

Supplemental Results:

Quality Control:
Zurich, Switzerland. One sample (11 October) was removed from analysis because the dilute sample (1:10) was below LOQ and the undilute sample was inhibited, as defined by recovery of less than 80% of the synthetic SARS-CoV-2 RNA added in.

PMMoV concentrations were obtained for all dates except October 4. Mean (standard deviation) PMMoV loads were 16.5 (0.12) $\log_{10}$ (gc/day). All PMMoV loads fell within 3 standard deviations of the mean, consistent with a normal distribution, except on 29 October (16.1 $\log_{10}$ (gc/day)). The sample was subsequently removed from further analysis.

San Jose, California, USA. From San Jose Wastewater Treatment Plant (San Jose, California, USA), daily samples were collected and processed throughout. PMMoV concentrations were mean (standard deviation) 8.9 (0.20) $\log_{10}$ (gc/g-dry weight). On two days (03 January 2021, 18 February 2021), PMMoV concentrations exceeded the mean plus three times the standard deviation. On one day (19 March 2021), PMMoV concentrations fell below the mean minus three times the standard deviation. These three samples were excluded from further analysis. All samples met criteria for inclusion based on BCoV concentrations, which were all greater than 10% of the expected concentrations based on the amount added.

Supplemental Materials and Methods:

Primer and Probe Design for SARS-CoV-2 S, N, and ORF1a genes (San Jose)
The assays used to detect SARS-CoV-2 S, N, and ORF1a genes in San Jose were designed using Primer3Plus (https://primer3plus.com/) based on the genome of the severe acute respiratory syndrome coronavirus 2 isolate Wuhan-Hu-1 (Accession Number MN908947.3). The assay was designed to target product size range of 60-200 bp at concentration of dNTPs of 0.8 mM and concentration of divalent cations of 3.8 mM, based on the following optimum (range) conditions: primer size: 20bp (15bp, 36bp); primer melting temperature 60℃ (50℃, 65℃); primer GC content: 50% (40%, 60%); hydrolysis probe size 20bp (15bp, 27bp); hydrolysis probe melting temperature 63℃ (62℃, 70℃); hydrolysis probe GC content: 50% (30%, 80%). The location (length) of the amplicons for N is 28287-28457 (171 bp), S is 23591-23665 (75 bp), and ORF1a is 12885-13063 (179 bp). Cross-reactivity was determined *in silico* using NCBI Blast. The assays were optimized by varying annealing temperature, and benchmarked against a respiratory virus verification panel using extracted RNA. Limit of the Blank was determined using negative nasal swab samples.

dPCR Mastermix and Thermocycling Conditions.
Zurich, Switzerland. Digital RT-PCR was performed on 5 µl template on either the Bio-Rad QX200 Droplet Digital (01 September 2020 - 17 October 2020) with the One-Step RT-ddPCR Advanced Kit for Probes (Bio-Rad CN 1864021) or Crystal Digital PCR using the Naica System (Stilla Technologies, 18 October - 20 January 2021) with the qScript XLT 1-Step RT-PCR Kit (QuantaBio CN 95132-500). SARS-CoV-2 N1 and N2 markers for the N gene were detected using the 2019-nCoV CDC ddPCR Triplex Probe Assay (Assay ID dEXD28563542, Bio-Rad)

according to manufacturer's instructions. For samples processed on the Bio-Rad QX200, 20 µl reaction volumes were prepared in a pre-reaction volume of 22 µl consisting of 5.5 µl of template, 5.5 µl of Supermix, 2.2 µl of Reverse Transcriptase, 1.1 µl of DTT and 1.1 µl of 20x 2019-nCoV CDC ddPCR Triplex Probe Assay. Primers and probes are included in Table S4. Droplets were generated using the QX100 Droplet Generator (Bio-Rad). PCR was performed on the T100 Thermal Cycler (Bio-Rad) with the following protocol: hold at 25℃ for 3 minutes, reverse transcription at 50℃ for 60 minutes, enzyme activation at 95℃ for 10 minutes, 40 cycles of denaturation at 95℃ for 30 seconds and annealing and extension at 55℃ for 1 minute, enzyme deactivation at 98℃ for 10 minutes, and an indefinite hold at 4℃. Ramp rate was 2℃/second, and the final hold at 4℃ was at least 30 minutes to stabilize droplets. Droplets were analyzed using the QX200 Droplet Reader (Bio-Rad) and thresholding done on the QuantaSoft Analysis Pro Software (Bio-Rad, Version 1.0).

For samples processed on the Crystal Digital PCR, 25 µl reactions were prepared in 27 µl pre-reaction volumes for Sapphire Chips (Stilla Technologies CN C14012) consisting of 5.4 µl of template, 13.5 µl of 2x qScript XLT One-Step RT-PCR, and 1.35 µl of 20x 2019-nCov CDC ddPCR Triplex Probe Assay. Droplet production and PCR were performed on the Naica Geode with the following protocol: reverse transcription at 48℃ for 50 minutes, denaturation at 94℃ for 3 minutes, followed by 40 cycles of denaturation at 94℃ for 30 seconds, annealing and extension at 57℃ for 1 minute. Chips were read and analyzed on the Naica Prism3 using the Crystal Reader and Crystal Miner software (Stilla Technologies).

For the Bio-Rad QX200 samples with more than 12000 droplets with average partitioning volume of 1 nl was deemed acceptable. For the Stilla Crystal Digital PCR 15000 droplets with average 0.8 nl were deemed acceptable. The average (standard deviation) number of droplets observed in samples from QX200 was 15000 (2100) and for the Crystal Digital PCR excluding controls was 24000 (2000). Average copies per partition (relative uncertainty) was 8.7×10^{-3} (54%). Every thermal cycler run included one or more no template and positive controls. Samples were deemed successful if the NTCs in the run contained 2 or fewer positive droplets, and the positive controls contained 3 or more. Technical replicate variability was, on average, less than 20%. Inter-experimental variation was quantified as the coefficient of variation in the performance of the positive control (target concentration of 100 gc/reaction) across 87 experiments, and was less than 25%. Assays were only conducted in one laboratory, so reproducibility was not assessed.

PMMoV was quantified by RT-qPCR using RNA UltraSense™ One-Step Quantitative RT-PCR System (Applied Biosystems CN 11732927) on a LightCycler® 480 instrument (Roche Life Science, Switzerland) using previously reported primers and probes (Microsynth AG, Switzerland, Table S4) (61, 62). Samples were prepared in 25 µl reaction volumes consisting of 5 µl of template, 5 µl of 5x Ultrasense Mix, 4 µl of Bovine Serum Albumin (Sigma-Aldrich CN 05470-1G) at 2 mg/ml concentration, 1.25 µl of Reverse Transcriptase, and 2.25 µl of primer and probe at final concentrations of 400 nM and 200 nM, respectively. Primers and Probe are listed in Table S4. The RT-qPCR was run with the following program: reverse transcription at 55℃ for 60 minutes, denaturation at 95℃ for 10 minutes, followed by 45 cycles of denaturation

at 95℃ for 15 seconds, annealing and extension at 60℃ for 1 minute. PMMoV quantification was performed by comparison to synthetic DNA standards (gBlock, IDT Technologies) run in duplicate at tenfold dilutions between $5x10^3$ and $5x10^7$ per 5 µl reaction. All thermal cycler runs were pooled for analysis.

San Jose, California, USA. Digital RT-PCR was performed on 20 µl samples from a 22 µl reaction volume, prepared using 5.5 µl template, mixed with 5.5 µl of One-Step RT-ddPCR Advanced Kit for Probes (Bio-Rad 1863021), 2.2 µl Reverse Transcriptase, 1.1 µl DTT and primers and probes at a final concentration of 900nM and 250nM respectively. Droplets were generated using the AutoDG Automated Droplet Generator (Bio-Rad). PCR was performed using Mastercycler Pro with the following protocol: reverse transcription at 50℃ for 60 minutes, enzyme activation at 95℃ for 5 minutes, 40 cycles of denaturation at 95℃ for 30 seconds and annealing and extension at either 59℃ (for SARS-CoV-2 assay) or 56℃ (for PMMoV/BCoV duplex assay) for 30 seconds, enzyme deactivation at 98℃ for 10 minutes then an indefinite hold at 4℃. The ramp rate for temperature changes were set to 2℃/second and the final hold at 4℃ was performed for a minimum of 30 minutes to allow the droplets to stabilize. Droplets were analyzed using the QX200 Droplet Reader (Bio-Rad), with thresholding done using QuantaSoft™ Analysis Pro Software (Bio-Rad, Version 1.0.596). The average (standard deviation) number of droplets in ten merged wells determined from a random subset of ten samples was 176000 (14500). Average (relative uncertainty) of the number of copies per partition (λ) in the same subset was $3.2x10^{-3}$ (52%). As the samples were extracted ten times and each extract analyzed in one well, technical replicate variability incorporates variation from both RNA extraction and RT-dPCR. Sample errors estimated from the merged wells were <10%, in line with coefficient of variation estimates of <8% for all three targets (S, N, ORF1a) in an experiment of replicate (n = 97) positive controls at target concentrations of 20 gc/µl. Assays were conducted in only one lab, so reproducibility was not assessed. Example fluorescence plots are provided in the associated reference by Topol et al. (58). All liquid transfers were performed using the Agilent Bravo (Agilent Technologies).